

Dissertation zur Erlangung des Doktorgrades
der Fakultät für Chemie und Pharmazie
der Ludwig-Maximilians-Universität München



**Targeting V-ATPase influences cancer cell
cholesterol metabolism and biophysical properties -
a new option for HCC therapy**

Karin Bartel

(geb. Steiner)

aus

München

2017

Erklärung

Diese Dissertation wurde im Sinne von § 7 der Promotionsordnung vom 28. November 2011 von Frau Prof. Dr. Angelika M. Vollmar betreut.

Eidesstattliche Versicherung

Diese Dissertation wurde eigenständig und ohne unerlaubte Hilfsmittel erarbeitet.

München, den 10.02.2017

Karin Bartel (geb. Steiner)

Dissertation eingereicht am 10.02.2017

1.Gutachterin Prof. Dr. Angelika M. Vollmar

2.Gutachterin PD Dr. Johanna Liebl

Mündliche Prüfung am 29.03.2017

To my family

CONTENTS

CONTENTS	4
SUMMARY	9
1. INTRODUCTION	12
1.1. Hepatocellular carcinoma.....	12
1.1.1. Risk factors and therapy options	12
1.1.2. Biomarkers and new strategies for treatment	13
1.2. The V-ATPase in light of cancer treatment	13
1.2.1. Physiological structure and function of the V-ATPases	13
1.2.2. The V-ATPase in cancer.....	15
1.2.3. V-ATPase inhibitors	15
1.3. Cholesterol metabolism.....	16
1.3.1. Cellular cholesterol homeostasis	17
1.3.2. Cholesterol - an integral membrane molecule with multiple functions ...	18
1.3.3. Implication of cholesterol metabolism in cancer	19
1.4. Oncogenic Ras signaling in HCC	19
1.5. Aim of the study	21
2. MATERIALS AND METHODS	23
2.1. Materials	23
2.1.1. Compounds	23
2.1.2. Inhibitors, reagents and technical equipment	23
2.1.3. Technical equipment	25
2.2. Methods	26
2.2.1. Cell culture solutions and media.....	26
2.2.2. Cell lines, maintenance and passaging	27
2.2.3. Freezing and thawing	28
2.2.4. Transient transfection with small-interfering RNA (siRNA)	28
2.2.5. Electroporation	28
2.2.6. CellTiter-Blue [®] cell viability assay.....	28
2.2.7. Crystal violet proliferation assay (Clonogenic Assay)	29
2.2.8. Immune fluorescence staining.....	29
2.2.9. Analysis of membrane polarity.....	30
2.2.10. Fluorescence recovery after photo-bleaching (FRAP).....	31

2.2.11. Cholesterol measurement.....	32
2.2.12. Cholesteryl ester analysis.....	32
2.2.13. Assessment of apoptosis.....	32
2.2.14. LDLR surface expression	33
2.2.15. Real-time deformability cytometry (RT-DC).....	33
2.2.16. Western Blot.....	34
2.2.17. Ras activity assay.....	38
2.2.18. Quantitative real-time PCR (qPCR).....	38
2.2.19. <i>In vivo</i> HUH-7 xenograft mouse model.....	39
2.2.20. Immune histochemistry (IHC).....	39
2.2.21. Statistical Analysis.....	40
3. RESULTS	42
3.1. V-ATPase inhibition induces cancer cell stiffening and alters membrane fluidity in HCC	42
3.1.1. Real-time deformability cytometry reveals cancer cell stiffening due to V-ATPase inhibition	42
3.1.2. V-ATPase inhibition induced cell stiffening due to alterations in membrane properties	44
3.2. V-ATPase inhibition alters cholesterol metabolism of HCC cells	47
3.2.1. Availability of free cholesterol is diminished upon V-ATPase inhibition .	47
3.2.2. V-ATPase inhibition impedes internalization of LDL via the LDLR and enhances LDLR expression.....	48
3.2.3. V-ATPase inhibition leads to cholesterol trapping and induction of <i>de novo</i> synthesis.....	51
3.3. Plasma membrane cholesterol depletion leads to impaired Ras signaling.....	53
3.3.1. Activation of the small GTPase Ras is impaired upon V-ATPase inhibition	53
3.3.2. Ras downstream signaling is altered upon treatment.....	55
3.4. A combination therapy approach to inhibit HCC proliferation.....	56
3.4.1. A combination of archazolid and simvastatin leads to synergistic growth inhibition of HCC cells <i>in vitro</i>	56
3.4.2. Archazolid strongly inhibits tumor growth in an <i>in vivo</i> mouse xenograft model.....	58

4. DISCUSSION.....	61
4.1. The V-ATPase influences membrane properties of the cell - and vice versa?	61
4.2. Cholesterol - an essential factor in cancer cell survival.....	63
4.3. Blocking cholesterol uptake and synthesis - a combination therapy as promising anti-cancer strategy	64
4.4. Inhibition of Ras signaling - new treatment option for an old oncogene	66
4.5. Concluding remarks and future perspectives	69
5. REFERENCES	72
6. APPENDIX.....	79
6.1. Abbreviations	79
6.2. Publications.....	82
6.2.1. Articles.....	82
6.2.2. Oral presentations	82
6.2.3. Poster presentations.....	82
6.3. Acknowledgements	84

SUMMARY

SUMMARY

Hepatocellular carcinoma (HCC) is one of the most frequent cancers worldwide and still a major cause of cancer-related death. Despite intensive research, therapy options are limited leaving an urgent need to develop new strategies. Recently, targeting cancer cell lipid and cholesterol metabolism came into focus especially in the context of HCC. Aberrantly increased cholesterol levels cause excessive proliferation, membrane-related mitogenic signaling and a reduction in cell stiffness - factors that favor tumor progression, malignancy and invasive potential. Yet, targeting cholesterol metabolism for cancer therapy is still challenging, leading to a sustained lack of effective therapy options. The V-ATPase inhibitor archazolid was recently implicated in cholesterol metabolism. We report for the first time a novel therapeutic potential of V-ATPase inhibition in cancer by influencing the mechanical phenotype of cancer cells thereby reducing oncogenic Ras signaling. Archazolid inhibits low density lipoprotein (LDL) uptake and induces lysosomal cholesterol trapping, which depletes free cholesterol from the cells and thus leads to an increase in cell stiffness and membrane polarity of cancer cells, while non-malignant hepatocytes remain unaffected. The deficiency of cholesterol in the plasma membrane decreases fluidity and leads to an inhibition of membrane-related Ras signaling resulting in decreased proliferation *in vitro* and *in vivo*. By simultaneous application of the lipid-lowering drug simvastatin, a well characterized inhibitor of *de novo* cholesterol synthesis, a potential escape mechanism by enhanced cholesterol production is prevented, thereby leading to a synergistic growth inhibition *in vitro*. Hence, we present a novel link between cell biophysical properties and proliferative signaling selectively in malignant HCC cells, which can be targeted synergistically by V-ATPase inhibition and blocking cholesterol synthesis, thus building the basis for an attractive and innovative strategy against HCC (Fig 1).

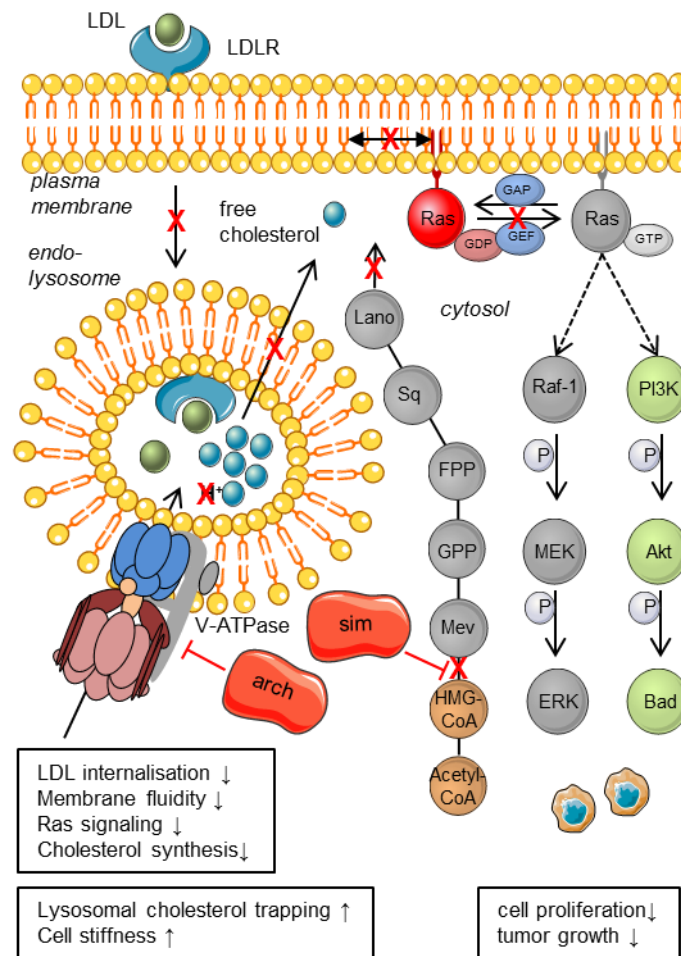


Figure 1 Effects of a combination therapy approach in HCC Upon inhibition of the V-ATPase by Archazolid (arch), LDLR internalization and acidification of the endo-lysosome is inhibited, causing subsequent accumulation of cholesterol within the lysosomes. Due to blocking the conversion of HMG-CoA to mevalonate by simvastatin (sim), *de novo* synthesis of free cholesterol is inhibited. The lack of free cholesterol leads to cholesterol depletion of the membrane and subsequently to disruption of cholesterol-enriched microdomains and a change in membrane properties. As a consequence, cholesterol microdomain-dependent Ras cannot be activated anymore and downstream signaling is inhibited, leading to reduced proliferation and tumor growth. Mev Mevalonate, GPP geranylpyrophosphate, FPP farnesylpyrophosphate, Sq squalene, Lano lanosterol, GEF guanosyl-exchange factor, GAP GTPase activating protein, LDL(R) low density lipoprotein (receptor)

INTRODUCTION

1. INTRODUCTION

1.1. Hepatocellular carcinoma

1.1.1. Risk factors and therapy options

Hepatocellular carcinoma (HCC) is the most common primary liver malignancy, one of the most frequent cancers worldwide and a major cause of cancer-related death (1-3). The global incident rate of HCC is disproportionate with an increased amount of cases in areas with a high occurrence of hepatitis infections and poor medical care. However, the frequency in the western world is constantly increasing, caused by migration from virus-endemic regions and changes in lifestyle promoting HCC risk factors (4).

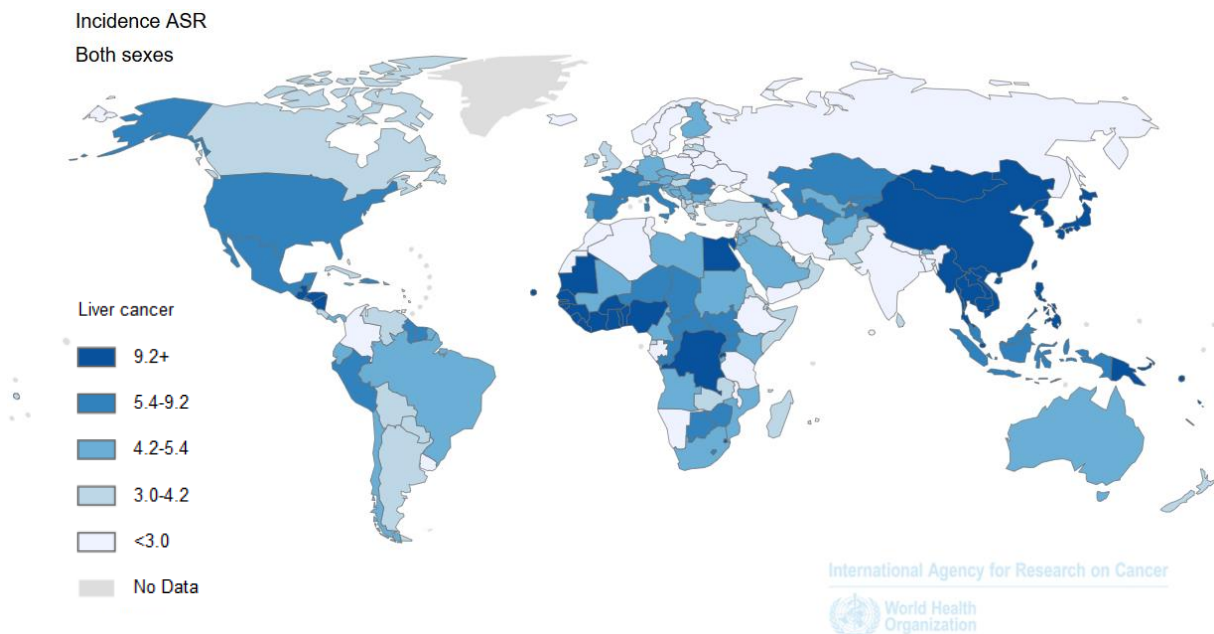


Figure 2 Global incidence of liver cancer Incidence of liver cancer in both sexes by geographical region. Age-standardized rate (ASR) of incidence is depicted in blue as a rate of new cases per 100,000 persons per year. Graphic sourced from GLOBOCAN 2012 (5).

The principal causes for the development of HCC are chronic liver diseases and cirrhosis, which are mainly promoted by infection with hepatitis B or C virus. Yet, besides viral hepatitis, alcohol consumption accounts for 40-50 % of HCC cases in Europe. Further conditions like diabetes, obesity, non-alcoholic fatty liver disease, smoking, aflatoxins, hereditary hemochromatosis or male sex increase the risk of developing the malignancy (2).

Despite intensive research, the prognosis remains poor, owing to late-stage diagnosis and limited therapy options. The first choices in treatment of early-stage HCC are liver transplantation and surgical resection; whereas the only approved systemic therapeutic option for late-stage HCC is the kinase inhibitor sorafenib, which extends the median overall survival by 2.8 months (6,7). Additionally, recurrence after transplantation and severe side effects of sorafenib display major problems in treatment.

1.1.2. Biomarkers and new strategies for treatment

In order to fight HCC, numerous studies are ongoing to reveal new therapeutic strategies and to improve diagnostic possibilities. A promising approach is focusing on the metabolic changes that lead to the malignancy, but also are caused by the disease. Several biomarkers have been proposed to serve for surveillance of high-risk patients in diagnosing HCC, such as serum concentrations of α -fetoprotein, des-gamma carboxythrombin, inflammation markers and many more (4). Several studies also report alterations in HCC lipid metabolism that might serve as biomarkers, especially deregulations in fatty acid oxidation and cholesterol metabolism have been observed (4,8). Targeting cancer lipid and cholesterol metabolism pathways has come into focus lately, as deregulation has been reported in various types of cancer cells and patient blood samples (9).

Interestingly, the vacuolar-type ATPase (V-ATPase), a protein in the focus of our research, has been implicated in cholesterol metabolism recently (10) and our group has already shown that V-ATPase inhibition displays anti-cancer properties (11-13). Hence, the V-ATPase seems to be an interesting new target in the treatment of HCC.

1.2. The V-ATPase in light of cancer treatment

1.2.1. Physiological structure and function of the V-ATPases

V-ATPases are large multi-subunit protein complexes expressed in a variety of cellular membranes, especially in the endo-lysosomal system. The V-ATPases are ATP-dependent proton pumps and are primarily responsible for maintaining pH homeostasis by regulation of the proton concentration in intracellular organelles. Basically, the V-ATPase consists of two functional domains (Fig 3): the V_1 domain, which is located at the cytosolic side of the membrane and exerts ATP hydrolysis to generate energy for the second domain, and the V_0 domain, which is integrated in the membrane and responsible for proton translocation (14,15). Both domains are

composed of a variety of different smaller subunits. In V_1 , the A and B subunits create the catalytic sites for ATP hydrolysis and the C-H subunits form central and peripheral stalk. Following energy generation, the V_0 domain moves in a rotatory fashion and protons bound to the domain can be released to the luminal side (14,16).

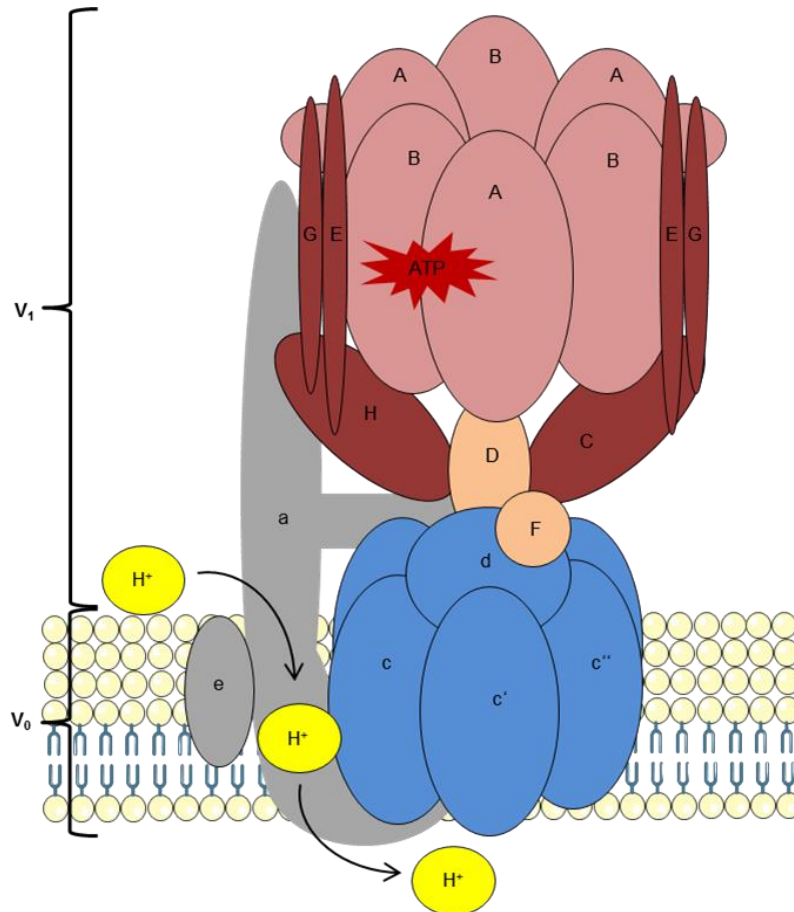


Figure 3 Structure of the V-ATPase The V-ATPase consists of two functional domains: the V_1 domain and the V_0 domain. The cytosolic V_1 domain is built by eight subunits A-F with A and B forming the catalytic sites for ATP hydrolysis (one site per AB heterodimer), C-H forming the peripheral stalk that keeps V_1 in its place and DF forming the central stalk which couples the energy to the V_0 domain. The membrane integral V_0 domain consists of subunits a,d,e and 4 copies of c. The c subunits form a membrane integral proteolipid ring and subunit a contains a hemichannel for proton (H^+) translocation. The proteolipid ring rotates subsequently to energy generation in V_1 domain, thereby enabling proton release to the luminal side. Illustration according to the model of Forgac et al. 2007 (14).

Consequentially to their function as proton pumps, V-ATPases play a crucial role in physiological processes like receptor-mediated endocytosis, membrane trafficking and recycling. Specialized cells also express the V-ATPase on their plasma membrane in order to acidify the extracellular space, important e.g. in the renal tube or in the process of bone resorption (14,17).

1.2.2. The V-ATPase in cancer

Expressing V-ATPase at the plasma membrane is also a feature reported for cancer cells. The extracellular space of tumors has been shown to display low pH provided by the V-ATPase, a metabolic status favoring migration and invasion of several cancer types including HCC. In this regard, V-ATPase expression at the plasma membrane was correlated with metastatic potential of cancer cells. (17-22)

Recently, the V-ATPase has emerged as promising anti-cancer target as inhibition leads to apoptosis induction of a variety of cancer cells. In this regard, our group could demonstrate that inhibition of epidermal growth factor receptor (EGFR) and transferrin receptor recycling by blocking V-ATPase function leads to an inhibition in cancer cell migration and induction of apoptotic cell death in highly metastatic cancer cells (11,12,23). Interestingly, Hamm et al. recently found first evidence that V-ATPase inhibition affects cholesterol homeostasis in cancer cells (24), a function that provides the possibility to be exploited for treatment of cancers relying on altered lipid metabolism.

1.2.3. V-ATPase inhibitors

As it has been shown that V-ATPase function is important for migration and survival of various cancer cells, inhibitors of the proton pump came into focus for anti-cancer therapies.

Since the early 1980s, the plecomacrolides bafilomycin and concanamycin which were isolated from *Streptomyces* species have been known to inhibit the V-ATPase. While bafilomycin was the first described inhibitor, concanamycin showed higher specificity. The plecomacrolides bind to the c subunit of the proteolipid ring thereby preventing rotation and proton translocation. (25,26) Further research in the late 1990s revealed the benzolactone enamides (e.g. salicylihalamide, apicularen) as inhibitors with IC₅₀ values in the nanomolar range (27). Efforts to simplify structures of V-ATPase inhibitors brought forth the synthetic indolyis, which are widely used for research due to the possibility of modification for different biophysical approaches (28,29).

Another highly potent inhibitor is archazolid (Fig 4), a myxobacterial secondary metabolite with IC_{50} values in the low nanomolar range. Archazolid was isolated from the strains *Archangium gephyra* and *Cystobacter violaceus* and its total synthesis has been published several years ago (30-33). Archazolid is a macrocyclic lactone that binds to the equatorial region of the c subunit thereby inhibiting rotation and proton translocation similar to plecomacrolides (27). As it is an inhibitor with high specificity and affinity as well as proven anti-cancer activity, we used it as a tool for studying

V-ATPase in HCC.

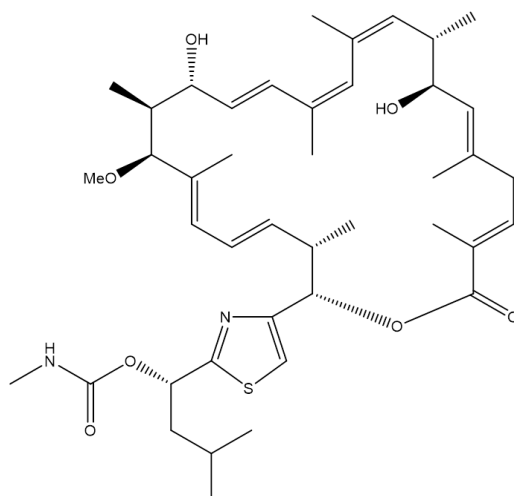


Figure 4 Structure of archazolid A adapted from Huss et al. 2009 (27).

1.3. Cholesterol metabolism

Cholesterol is a molecule of central importance in the human body and as such has been intensively studied for a long time. It is an essential component of the membrane barrier influencing its fluidity, the function of membrane proteins and transmembrane signaling processes (34). Furthermore, cholesterol is a precursor for steroids and bile acids, which have important biological roles in signal transduction and regulation of other lipids. Owing to its various functions, de-regulation in cholesterol homeostasis is implicated in many serious diseases like atherosclerosis, diabetes and cancer (34,35). Hence, cholesterol metabolism is extensively regulated.

1.3.1. Cellular cholesterol homeostasis

In principle, cellular cholesterol homeostasis is regulated by synthesis, influx and efflux. Eukaryotic cells can synthesize cholesterol in the endoplasmic reticulum (ER), utilizing the mevalonate pathway starting from Acetyl-CoA. The rate-limiting step of the *de novo* synthesis is the reduction of HMG-CoA to mevalonate catalyzed by the HMG-CoA reductase (HMGCR), the direct target of statins. (34-36) Apart from their indication as lipid-lowering agents, statins were also tested in several studies for the use as anti-cancer agents, but until now with controversial outcome (37,38).

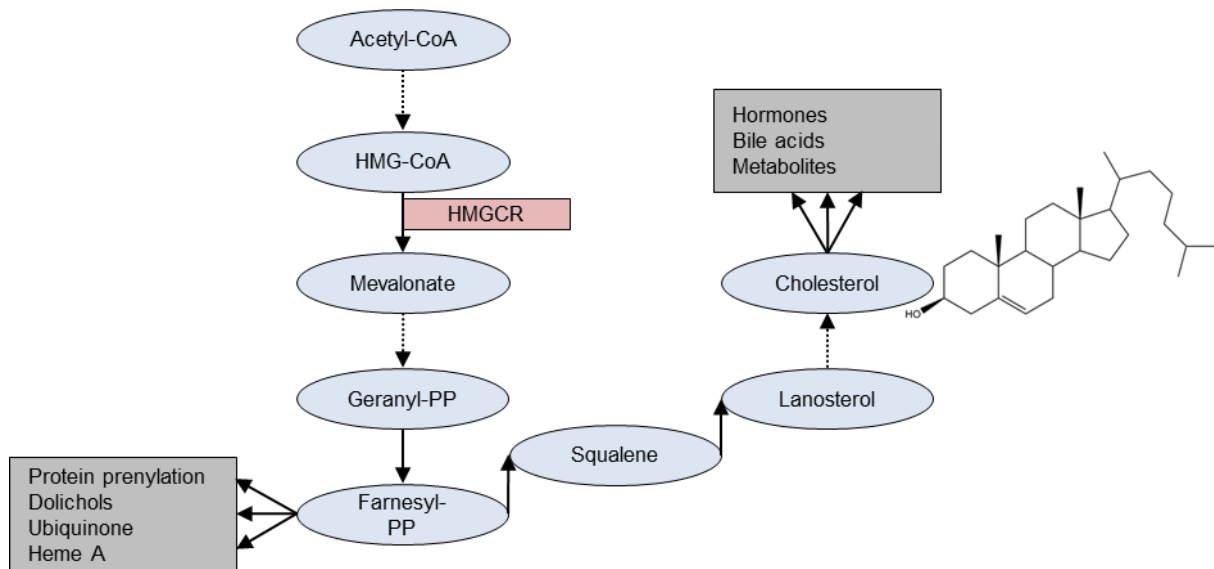


Figure 5 Cholesterol synthesis pathway Starting from Acetyl-CoA, HMG-CoA is synthesized via multiple enzymatic reactions. The subsequent reduction of HMG-CoA to mevalonate, catalyzed by the HMGCR, is the rate-limiting step of the following synthesis. After further multiple reactions, farnesyl-PP is synthesized, which is used to generate additional important metabolites with distinct cellular functions. Cholesterol is synthesized in a complex pathway facilitating demethylations and double bond reductions in about 20 different reactions from lanosterol. Cholesterol is then further metabolized or used as membrane building block. Illustrated according to Ikonen and Thurnher (34,36). Dashed lines between molecules (blue boxes) indicate multiple reactions; PP pyrophosphate; grey boxes list sequential functions and products.

The second important way for cells to increase their cholesterol content is the internalization of cholesterol-containing lipoproteins mainly via the low-density lipoprotein receptor (LDLR) pathway. Dietary cholesterol is absorbed in the small intestine and transported to hepatocytes that provide the body with very low-density lipoprotein (VLDL). In the circulation VLDL is processed to LDL, which can bind to the LDLR on the surface of cells. The complex is then internalized and cleaved in the

acidic environment of the endo-lysosomal system. The LDLR is recycled back to the cellular surface and free cholesterol is released into the cytosol. (35,39)

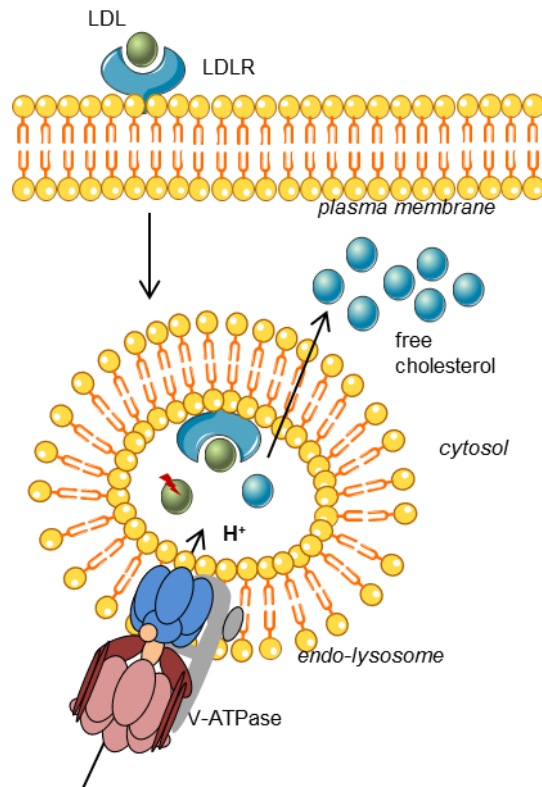


Figure 6 LDL internalization LDL (green) from the circulation binds to the LDLR on the outer surface of the plasma membrane. The complex is internalized into the endo-lysosomal system. In the acidic environment of the lysosome, created by the V-ATPase, LDL dissociates from the receptor, is cleaved and free cholesterol (blue) is released into the cytosol.

While excess cholesterol is esterified for intracellular storage or externalized, free cholesterol is further metabolized or integrated into membranes.

1.3.2. Cholesterol - an integral membrane molecule with multiple functions

Cholesterol is one of the main components of mammalian cell membranes with a molar proportion of up to 50 % in the plasma membrane (40). Probably the most important function of membrane cholesterol is to modulate biophysical properties by increasing order. Integration of cholesterol between phospholipids decreases mobility of phospholipids and raises the packing density within the membrane, thereby influencing mechanical strength and fluidity (41).

Yet, cholesterol is heterogeneously present within intracellular membranes, while 40-90 % of cellular free cholesterol is integrated into the plasma membrane, mitochondria for instance only contain about 0.5-3 % of the cholesterol concentration

and golgi membranes show intermediate levels (41-43). This indicates additional functions for membrane cholesterol.

There exist small areas within membranes that are especially rich in cholesterol and sphingolipids and display a very high membrane order, the lipid-rafts. These distinct microdomains also contain transmembrane and membrane-integrated proteins essentially involved in signal transduction. (44,45) Lipid-rafts have been shown to regulate activity of enzymes and to influence ion channels and membrane receptors, thereby modulating proliferation and signaling (40,41,45,46).

1.3.3. Implication of cholesterol metabolism in cancer

Given the functions of cholesterol, it is not surprising that alterations in cholesterol metabolism have been shown both to occur in and to influence cancer cells. Cholesterol is an important player in the development of malignancy. High cholesterol levels in cancer cells are known to be beneficial for tumor progression and drug resistance and it has been reported that alterations in cholesterol levels of primary tumor cells and HCC cell lines were linked with chemotherapy resistance and protection from apoptosis (9,47).

Lately, increasing evidence suggests that the loss of cell stiffness correlates with the malignancy and invasive potential of cancer cells. Studies have shown that cancer cells are softer than their non-malignant counterparts, which seems to correlate with metastasis, invasion and tumor stage (40,46). Furthermore evidence increases that de-regulated cholesterol metabolism in cancer cells influences intracellular signaling (48,49). Cholesterol metabolism therefore emerged as a promising target in the combat to find new anti-cancer treatment options.

1.4. Oncogenic Ras signaling in HCC

The small GTPase Ras is a well-known oncogene mutated in 20 % of all tumors, and has been shown to be an oncogene excessively activated in HCC (50,51). Interestingly, recent research suggests that cholesterol content of the plasma membrane influences signaling pathways, like e.g. Ras signaling, and therefore might be of interest when considering aberrant Ras signaling in cancer (52).

In HCC, genetic mutations in Ras or the downstream effector Raf are rare compared to other tumor types; however activation of the Ras downstream pathways commonly occurs through dysregulation of Ras activators or inhibitors (53,54). In general, increased activity of Ras displays poor prognosis for cancer patients.

The activation state of Ras is dependent on the binding status of guanosine diphosphate (GDP) or guanosine triphosphate (GTP). Inactive Ras is bound to GDP, which is exchanged for GTP by guanosyl-exchange factors (GEFs) such as SOS. Activation of GEFs is for example facilitated by the binding of growth factors to their receptor on the cell surface. GEFs are then recruited to the plasma membrane to activate Ras. GTP-bound Ras in turn activates various downstream signaling cascades like the MAPK or PI3K pathway, which ultimately lead to transcription of cell proliferation-, migration-, survival-, differentiation- and mesenchymal-epithelial-transition-related target genes (50,53).

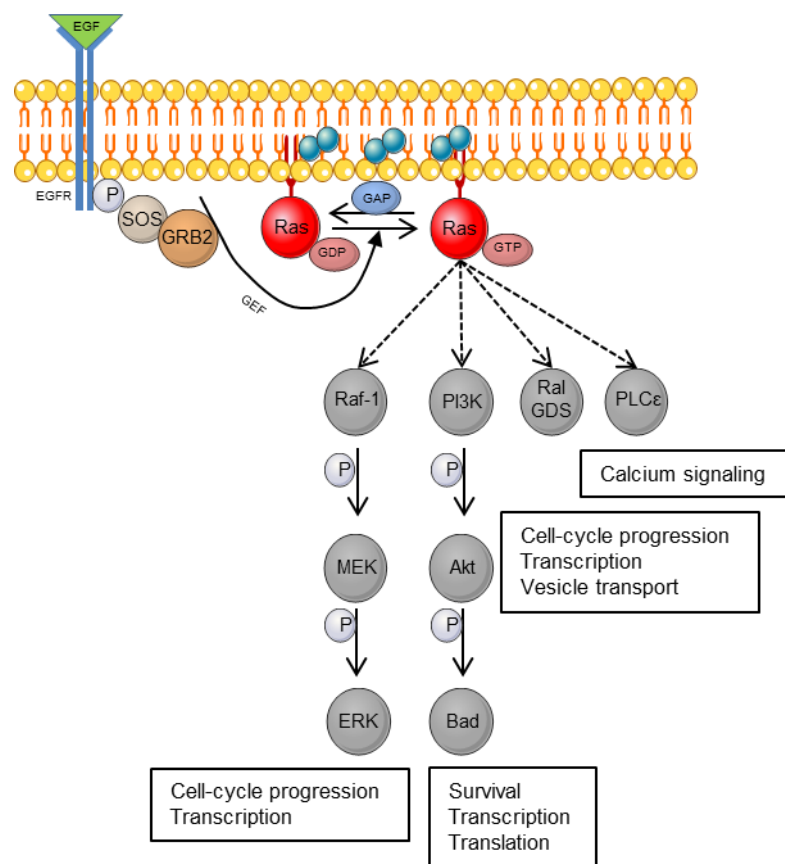


Figure 7 Activation of Ras downstream signaling Upon binding of a growth factor like EGF to its respective receptor on the cell surface, receptor downstream signaling is initiated. In case of the EGF, the receptor dimerizes and undergoes autophosphorylation. Subsequently, the guanosyl-exchange factor (GEF) SOS and the adapter protein GRB2 are recruited. GEFs exchange GDP bound to Ras for GTP, which leads to an activation at cholesterol-rich membrane sites. Activated Ras in turn activates various downstream signaling pathways that lead to distinct functions, as depicted in the respective boxes. Deactivation of Ras is facilitated by GTPase activating proteins (GAPs) that exchange GTP for GDP. Blue circles represent cholesterol. Illustration adapted from Delire et al. 2015 and Downward et al. 2013 (50,53).

1.5. Aim of the study

Our group has previously introduced the potent V-ATPase inhibitor archazolid as an interesting and effective anti-cancer agent and unraveled different aspects of its mechanism of action (11-13,23). Interestingly, there is initial evidence now that V-ATPase inhibition affects cholesterol homeostasis in cancer cells (24).

In the present study we aim to specifically target cancer cell cholesterol metabolism by archazolid single treatment and furthermore in a combination therapy approach together with simvastatin. We want to

- analyze the effect of V-ATPase inhibition on cell biophysical properties
- investigate the role of V-ATPase in cholesterol regulation
- assess possible consequences on cell survival
- and reveal underlying mechanisms

in order to find new strategies for the treatment of HCC (Fig 8).

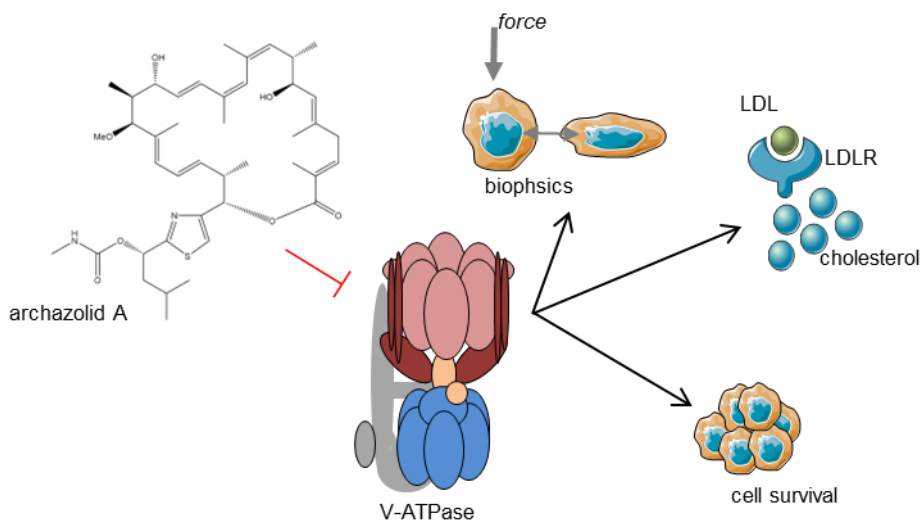


Figure 8 Study objectives The study aims to use archazolid A as a tool to investigate the influence of V-ATPase inhibition on cellular biophysics, cholesterol metabolism and cell survival in order to find new treatment strategies for HCC.

MATERIALS AND METHODS

2. MATERIALS AND METHODS

2.1. Materials

2.1.1. Compounds

The myxobacterial compound archazolid A was provided by Rolf Müller (Saarland University) and simvastatin was purchased from Sigma-Aldrich. The compounds were dissolved to 10 mM stock solutions in DMSO and stored at -20 °C. As the final DMSO concentration in the experiments did not exceed 0.1 %, possible DMSO side effects could be excluded.

2.1.2. Inhibitors, reagents and technical equipment

Table 1 Biochemicals, dyes, inhibitors, kits and cell culture reagents

Reagent	Producer
5x siRNA Buffer	Dharmacon™, GE Healthcare, USA
Amaxa™ Cell Line Nucleofector™ Kit T	Lonza Cologne AG, Cologne, Germany
Amplex® Red Cholesterol Assay Kit	Molecular Probes Inc., Thermo Fisher, Eugene, OR, USA
BC Assay reagent	Interdim, Montulocon, France
Bovine serum albumin	Sigma-Aldrich, Taufkirchen, Germany
Cell-Titer Blue™	Promega, Madison, WI, USA
Collagen A/G	Biochrom AG, Berlin, Germany
Complete® EDTA free	Roche Diagnostics, Penzberg, Germany
Crystal violet	Carl Roth, Karlsruhe, Germany
Dithiotherithol (DTT)	AppliChem, Darmstadt, Germany
Dulbecco's Modified Eagle Medium (DMEM)	PAA Laboratories, Pasching, Austria
DMSO	Sigma-Aldrich, Taufkirchen, Germany
EDTA	Carl Roth, Karlsruhe, Germany
EGTA	Sigma-Aldrich, Taufkirchen, Germany
EGF	Peptotech, Rocky Hill, USA
FCS	Biochrom AG, Berlin, Germany

FluorSave™ Reagent	Merck, Darmstadt, Germany
Formaldehyde 16 %, ultrapure	Polysciences, Eppelheim, Germany
GlutaMAX™	Life Technologies, Thermo Fisher, Carlsbad, CA, USA
HepaRG™ Thaw, Plate, & General Purpose Medium Supplement	Life Technologies, Thermo Fisher, Carlsbad, CA, USA
HepaRG™ Maintenance/Metabolism Medium Supplement	Life Technologies, Thermo Fisher, Carlsbad, CA, USA
High-Capacity cDNA Reverse Transcription Kit	Applied Biosystems, Foster City, CA, USA
Hoechst 33342	Sigma-Aldrich, Taufkirchen, Germany
Igepal CA 630 (Nonidet P 40)	Sigma-Aldrich, Taufkirchen, Germany
Na ₃ VO ₄	ICN Biomedicals, Aurora, Ohio, USA
NaCl	Sigma-Aldrich, Taufkirchen, Germany
NaF	Merck, Darmstadt, Germany
Non-fat dry milk powder (Blotto)	Carl Roth, Karlsruhe, Germany
Page-Ruler™ Prestained Protein Ladder	Fermentas, St. Leon-Rot, Germany
Penicillin/Streptomycin (P/S)	PAA Laboratories, Pasching, Austria
PFA	Sigma-Aldrich, Taufkirchen, Germany
PMSF	Sigma Aldrich, Taufkirchen, Germany
Polyacrylamid	Carl Roth, Karlsruhe, Germany
PowerUp™ SYBR Green Master Mix	Applied Biosystems, Foster City, CA, USA
Propidium iodide	Sigma-Aldrich, Taufkirchen, Germany
Qiagen RNeasy Mini Kit	Qiagen, Hilden, Germany
Ras Activation Kit ab128504	Abcam, Cambridge, UK
Sodiumdodecylsulfate (SDS)	Carl Roth, Karlsruhe, Germany
TCE	Sigma-Aldrich, Taufkirchen, Germany
Tris Base/HCl	Sigma-Aldrich, Taufkirchen, Germany
Trisodium citrate dicydrate	Sigma-Aldrich, Taufkirchen, Germany
Triton X-100	Merck, Darmstadt, Germany
Trypsin	PAN Biotech, Aidenbach, Germany
Tween 20	Bio-Rad, Munich, Germany
VECTASTAIN Elite ABC HRP Kit	Vectorlaboratories, Burlingame, CA,

(Peroxidase, Universal)	USA
ImmPACT AEC Peroxidase (HRP)	Vectorlaboratories, Burlingame, CA,
Substrate	USA
William's E-Medium	Life Technologies, Thermo Fisher,
	Carlsbad, CA, USA

2.1.3. Technical equipment

Table 2 Technical equipment

Technical equipment	Producer /Distributor
7300 Real Time-PCR System	applied Biosystems, ThermoFisher PCR, Scientific, Waltham, MA, USA
Axiovert 25	Zeiss, Oberkochen, Germany
BD FACS Canto™ II	BD Biosciences, Heidelberg, Germany
Canon EOS 450C camera	Canon, Tokyo, Japan
ChemiDoc™ Touch Imaging system	Bio-Rad, Hercules, CA, USA
Consort Electrophoresis Power Supply E835	Sigma-Aldrich, Taufkirchen, Germany
Curix 60	Agfa, Cologne, Germany
ibiTreat μ-slide 8-well	ibidi GmbH, Munich, Germany
Leica-SP8 confocal microscope	Leica Microsystems Inc., IL, USA
Mikro 22R centrifuge	Hettich, Tuttlingen, Germany
Mini-PROTEAN 3	Bio-Rad, Munich, Germany
Nanodrop® ND-1000	Peqlab, Wilmington, DE, USA
Nucleofector™II Device	Lonza, Basel, Switzerland
Odyssey 2.1	LI-COR Biosciences, Lincoln, NE, USA
Olympus CK30 and BX41	Olympus Deutschland GmbH, Hamburg, Germany
Primus 25 advanced® Thermocycler	PeQlab, Erlangen, Germany
PVDF Blotting Membrane 0,2 μm	Amersham™ Hybond™, GE Healthcare, Life science, Germany
QuantStudio® 3 Real-Time Instrument (96-Well 0.1 ml Block)	applied biosystems, ThermoFisher PCR, Scientific, Waltham, MA, USA
Rotational Vacuum Concentrator RVC	Martin Christ Gefriertrocknungsanlagen

2-18	GmbH, Osterode am Harz, Germany
SpectraFluor Plus™	Tecan, Männedorf, Switzerland
Suprafuge 22	Heraeus Sepatch, Osterode am Harz, Germany
Thermoshake, Laboshake	Gerhard Analytical Systems, Königswinter, Germany
Top stage incubator	Oko Lab, Ottaviano, Italy
Ultrasonic cleaner	VWR International GmbH, West Chester, PA, USA
Vi-Cell™ XR	Beckman Coulter, Brea, CA, USA
Zeiss LSM 510 Meta confocal laser scanning microscope	Zeiss, Oberkochen, Germany

2.2. Methods

2.2.1. Cell culture solutions and media

The following solutions and reagents were used for cultivation and maintenance.

Table 3 Cell culture solutions and media

PBS (pH 7.4)		PBS + Ca²⁺/Mg²⁺ (pH 7.4)	
NaCl	132.2 mM	NaCl	137 mM
Na ₂ HPO ₄	10.4 mM	KCl	2.68 mM
KH ₂ PO ₄	3.2 mM	Na ₂ HPO ₄	8.10 mM
in H ₂ O		KH ₂ PO ₄	1.47 mM
		MgCl ₂	0.25 mM
		CaCl ₂	0.5 mM
		in H ₂ O	
DMEM++		Trypsin/EDTA (T/E)	
DMEM	500 ml	Trypsin	0.5 %
FCS	10 %	EDTA	0.20 %
P/S	1 %	in PBS	

Collagen G

Collagen G	0.001 %
in PBS	

FCS was inactivated by partially thawing for 30 min at room temperature, totally thawing at 37 °C and finally incubating at 56 °C for 30 min. FCS aliquots were stored at -20 °C.

2.2.2. Cell lines, maintenance and passaging

HUH7 and HepG2 cells were obtained from Japanese Collection of Research Bioresources (JCRB) and German Research Centre of Biological Material (DSMZ) (ACC180), respectively. Cell line STR profiling was performed. HCC cells were grown in DMEM++. HepaRG™ cells were obtained from Life Technologies. Cells were plated and maintained in Williams' medium E supplemented with GlutaMAX™ and HepaRG™ Thaw, Plate, & General Purpose Medium Supplement (Thaw, Plate, & General Purpose Working Medium) purchased from Life Technologies. For metabolism studies, cells were seeded in Thaw, Plate, & General Purpose Working Medium, which was replaced by in Williams' medium E supplemented with GlutaMAX™ and HepaRG™ Maintenance/Metabolism Medium Supplement (Metabolism Medium) after 24 h. Thereafter medium was renewed every 3 days. Experiments were performed after 7 days of cell maintenance in Metabolism Medium. Primary human hepatocyte tissue samples (hHep) and annotated data were obtained and experimental procedures were performed within the framework of the non-profit foundation HTCR, including the informed patient's consent. For experiments hHep were cultivated in DMEM++. All cells were cultured under constant humidity at 37 °C and with 5 % CO₂ in an incubator. All culture flasks, multiwell-plates and dishes were first coated with collagen G before seeding the cells. Cells were routinely tested for contamination with mycoplasma using PCR detection kit VenorGeM (Minerva Biolabs).

After reaching confluency, growth medium was removed, cells were washed twice with pre-warmed PBS and detached by incubation with pre-warmed T/E for approximately 5 min at 37 °C. Digestion was stopped by adding 10 ml growth medium, cells were centrifuged (1000 rpm, 5 min), resuspended in medium, counted and plated for the respective experiments. All plates and dishes were pre-coated with

collagen G for better adhesion and cell function. Cell concentration and viability were determined using Vi-Cell™ XR cell viability analyzer (Beckman Coulter).

2.2.3. Freezing and thawing

For long-term storage, cells were detached, counted and 2×10^6 HCC cells or 4×10^6 HepaRG™ were resuspended in 1 ml growth medium supplemented with 20 % FCS, 1 % P/S and 20 % DMSO. Cells were transferred into cryo vials and immediately frozen at -20 °C for 24 h, transferred to -80 °C for at least 6 h and finally to liquid nitrogen for long-term storage. For thawing, the frozen cells were warmed up in a water bath to 37 °C and transferred into 5 ml growth medium. The cells were pelleted and the supernatant was discarded to remove DMSO. Subsequently cells were resuspended in growth medium and placed into a 25 cm² culture flask. The following day, growth medium was changed and the cells were left to reach confluency.

2.2.4. Transient transfection with small-interfering RNA (siRNA)

For silencing experiments, cells were seeded 24 h prior to transfection with siRNA using DharmaFECT™ transfection reagents and manufacturer's protocol (Dharmacon™, GE Healthcare). The c-subunit of the V-ATPase (ATP6V0C) was silenced using ON-TARGETplus SMARTpool siRNA (2 µg) and non-targeting siRNA (nt siRNA) as a control (Dharmacon™, GE Healthcare). 48 h after transfections cells were harvested for the respective assay.

2.2.5. Electroporation

Plasmid transfection was performed by electroporation according to manufacturer's instruction using Amaxa™ Cell Line Nucleofector™ Kit T. In brief, cells were detached, counted and 2×10^6 cells were transferred into a tube, centrifuged and the supernatant was discarded. The cells were resuspended in 100 µl Nucleofector™ solution and 2 µg plasmid were added. The cell suspension was transferred into a cuvette and transfected using the T-28 program. The transfected cells were transferred into medium and plated for the respective assay.

2.2.6. CellTiter-Blue® cell viability assay

The metabolic capacity of cells can be considered as an indicator for their viability. To analyze viability, the CellTiter-Blue® cell viability assay (Promega) was employed, which uses the indicator dye resazurin.

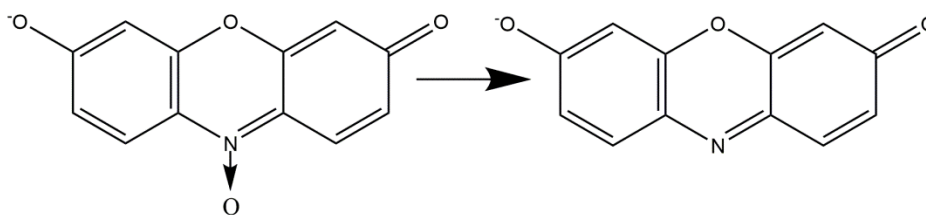


Figure 9 CellTiter-Blue® cell viability assay reaction In viable cells resazurin (left) is reduced to resorufin (right), which shows fluorescence at 590 nm.

Therefore 5,000 cells/well were seeded into 96-well plates and allowed to adhere overnight. Before stimulation initial metabolic activity was determined and cells were treated as indicated for 72 h. 4 h before end of stimulation time CellTiter-Blue® Reagent was added and the fluorescence at 590 nm was measured with the SpectraFluor Plus™ plate reader. The fluorescence is proportional to the cell number.

2.2.7. Crystal violet proliferation assay (Clonogenic Assay)

For the evaluation of long-term effects on proliferation of HUH7 cells, a clonogenic assay was performed. HUH7 cells were seeded, left to adhere for 24 h and treated as indicated for 24 h. After stimulation time, cells were detached and reseeded at a density of 10,000 cells/well on a 6-well plate. After 7 days cells were stained with 1 ml 0.5 % crystal violet solution for 10 min at room temperature. After removal of the dye and five washing steps with distilled water, cells were imaged at 10x magnification. Subsequently, 1 ml dissolving buffer/well was added and absorbance at 550 nm was measured with the SpectraFluor Plus™ plate reader.

Table 4 Clonogenic assay solutions

Crystal violet solution		Dissolving buffer	
Crystal violet	5 % (w/v)	Trisodium citrate	20 mM
Methanol	20 %	Ethanol	50 %
in H ₂ O		in H ₂ O	

2.2.8. Immune fluorescence staining

To stain HUH7 cells for confocal microscopy 20,000 cells/well were seeded on ibiTreat μ-slide 8-well slides one day prior to treatment as indicated. After treatment, cells were washed with PBS, fixed with 3 % Paraformaldehyde (PFA) for 30 min, permeabilized with 0.1 % triton-X and unspecific binding was blocked with 2 % BSA.

Subsequently, the proteins of interest were bound with specific antibodies for 2 h at 25 °C or at 4 °C overnight and visualized with fluorescent secondary antibodies for 45 min at 25 °C. Cholesterol was stained with 50 µg/ml filipin (Sigma Aldrich) for 2 h at 25 °C. Nuclei were stained with TO-PRO®3 or Hoechst. Actin was stained with rhodamine-phalloidin. Cells were washed and mounted with FluorSave™ Reagent mounting medium and covered with a glass coverslip. Images were taken by confocal microscopy.

Table 5 Primary antibodies for confocal microscopy

Antigen	Company	Cat. No.
LAMP-1	Developmental Studies Hybridoma Bank	H4A3
LDLR	Santa Cruz	sc-18823

Table 6 Secondary antibodies and dyes for confocal microscopy

Antigen	Company	Cat. No.
Mouse IgG (AlexaFluor 488 conjugate)	Life Technologies	A - 11001
TO-PRO®3	Life Technologies	T3605
Filipin	Sigma Aldrich	F4767
di-4-ANEPPDHQ	Life Technologies	D36802
Rhodamine-Phalloidin	Life Technologies	R-415
DiLDL	Life Technologies	L3482
Hoechst 33342	Sigma Aldrich	H6024

2.2.9. Analysis of membrane polarity

For analysis of membrane polarity, 20,000 cells/well were seeded on ibiTreat µ-slide 8-well slides 24 h prior to stimulation. The cells were treated as indicated for 24 h. Subsequently, medium was exchanged for DMEM without FCS containing 10 µM of the dye di-4-ANEPPDHQ for 30 min at 37 °C. Live cell imaging was performed as described previously using a Leica TCS SP 8 SMD confocal microscope with a top stage incubator (Oko Lab, Ottaviano, Italy). In brief, the dye intercalates into membranes and changes its emission spectrum due to polarity of the environment. By calculating the ratio (generalized polarization, GP) of light intensities between the channels membrane polarity can be analyzed.

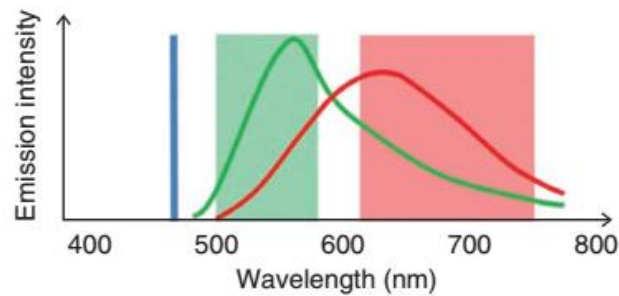


Figure 10 Fluorescence properties of di-4-ANEPPDHQ After excitation at 488 nm (blue line), the dye fluoresces either with a peak emission around ~560 nm (green line) when residing in less polar environment, or at ~620 nm in the rather polar disordered phase (red line). Both wavelength bands indicated by the shaded boxes are detected by two channels. Image adapted from Owen et al. (55).

For analysis of the images a macro for ImageJ (ImageJ 1.46r, NIH, USA) based on the one provided by Owen et al. (55) was used designed with the kind help of Erwin Steiner. Statistical evaluation of GP value distribution was performed with GraphPad Prism.

2.2.10. Fluorescence recovery after photo-bleaching (FRAP)

24 h prior to treatment as indicated, HUH7 cells were transfected with a plasmid coding for farnesylated GFP (pAcGFP1-C1, Clontech). Electroporation using Amaxa® Cell Line Nucleofector® Kit T (program T-28) as described in 2.2.5 was employed. 40,000 cells per well were subsequently seeded onto ibiTreat μ -slide 8-well slides and FRAP assay was performed using a Leica TCS SP 8 SMD confocal microscope with a top stage incubator (Okolab). A defined region of interest was bleached with high laser power and recovery of the GFP signal was monitored by recording 60 post bleach images every 10 s.

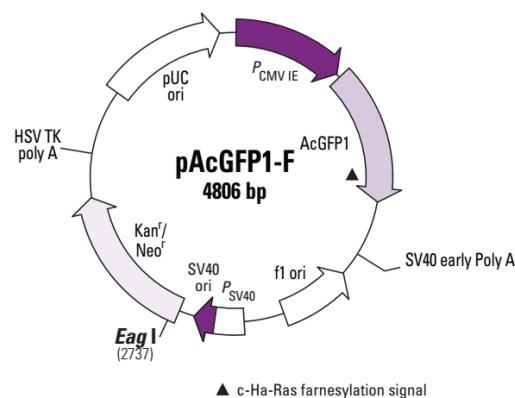


Figure 11 Plasmid vector information for pAcGFP1-F Adapted from manufacturer's product information (Catalog No. 632511 pAcGFP1-F, Clontech, CA, USA).

2.2.11. Cholesterol measurement

Cellular cholesterol levels were measured using the Amplex® Red Cholesterol Assay Kit according to manufacturer's protocol. The assay is based on an enzyme-coupled reaction that detects both free cholesterol and esterified cholesterol by generating H₂O₂ that is subsequently detected using 10-acetyl-3,7-dihydroxyphenoxazine (Amplex® Red reagent). Therefore, cells were treated as indicated for 48 h, detached and either homogenized right away in a lipid extraction solution containing chloroform, isopropanol and IGEPAL CA-630 (7:11:0.1) via sonication, or homogenization was performed on lysosomes isolated as described previously (56). After centrifugation (13,000x g, 10 min) the organic phase was air dried at 50 °C for 10 min to remove chloroform. Remaining organic solvent was removed by vacuum at 30 °C for 30 min. Dried lipids were dissolved in 1x assay reaction buffer and mixed 1:1 with a working solution containing 300 µM Amplex® Red reagent, 2 U/ml horseradish peroxidase (HRP), 2 U/ml cholesterol oxidase and in case of total cholesterol measurement 0.2 U/ml cholesterol esterase. After incubation for 30 min at 37 °C fluorescence was measured with the SpectraFluor Plus™ plate reader.

2.2.12. Cholesteryl ester analysis

HUH-7 cells were treated as indicated, trypsinized and collected by centrifugation. The cell pellet was frozen in liquid nitrogen and stored at -80 °C until use. The pellet was resuspended in methanol, chloroform was added and finally PBS. Cells were then centrifuged at 4000 rpm for 5 min and lower chloroform phase was collected. The chloroform was evaporated for 20 min at 30 °C and dried lipids were dissolved in methanol. After centrifugation at 1500 rpm for 5 min, supernatant was diluted with methanol, centrifuged again at 1500 rpm for 5 min and analysed by LC-MS/MS, as described previously (57).

2.2.13. Assessment of apoptosis

Apoptosis was analyzed according to the method described by Nicoletti et al. (58). In this assay, the subG1 population, which is characteristic for DNA fragmentation and loss of nuclear DNA, is evaluated. For this purpose, cells were detached, washed with PBS and resuspended in 100 µl flow cytometry solution, containing propidium iodide (PI) and incubated for 30 min at 4 °C. Apoptotic DNA was determined by flow cytometry using BD FACS Canto™ II. For data evaluation the flow cytometry analysis software FlowJo 7.6 was employed.

Table 7 Flow cytometry solution

Flow cytometry solution	
Propidium iodide	75 μ M
Trisodium citrate	0.1 %
Triton-X 100	0.1 %
in PBS	

2.2.14. LDLR surface expression

Cells were treated as indicated for 24 h. After stimulation, growth medium was removed and the cells were washed twice with pre-warmed PBS before trypsination, washed again with PBS once and incubated with anti-LDLR antibody (sc-18823, santa cruz) for 45 min at room temperature. After washing, secondary antibody conjugated to AlexaFluor 488 was added for 45 min at room temperature and after two additional washing steps, cells were analyzed by flow cytometry with a FACSCanto II cytometer.

2.2.15. Real-time deformability cytometry (RT-DC)

For RT-DC measurements the experimental setup has been described earlier (59). Cells were trypsinized and resuspended to a final concentration of about 3×10^6 cells/ml in 0.5 % methylcellulose solved in PBS. To achieve cell deformation the cell suspension was pumped through a microfluidic chip containing a constricted channel of $30 \mu\text{m} \times 30 \mu\text{m}$ at flow rates of 0.16 $\mu\text{l/s}$, 0.24 $\mu\text{l/s}$ and 0.32 $\mu\text{l/s}$.

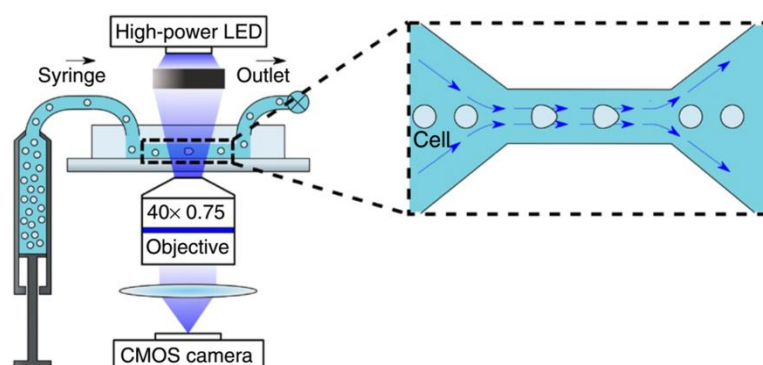


Figure 12 Schematic setup of RT-DC assay setup Image adapted from Otto et al. (59).

As a reference, non-deformed cells were measured outside the channel in the reservoir where cell deformation does not take place. Cell size (cross-sectional area) and deformation ($1 - \text{circularity}$) was determined in real-time for >3000 cells per

experiment at rates of 100 cells/sec. Isoelasticity lines were assessed as reported elsewhere (60).

$$RD = \frac{(d_{chan}^{treat} - d_{res}^{treat})}{(d_{chan} - d_{res})}$$

Figure 13 Calculation of relative deformation RD relative deformation, $d(\text{treat-chan})$ deformation of the treated samples in the channel, $d(\text{treat-res})$ deformation of the treated samples in the reservoir, $d(\text{chan})$ deformation of the control samples in the channel, $d(\text{res})$ deformation of the control samples in the reservoir

Statistical analysis was performed by applying linear mixed effects models. Therefore, a fixed effects model is extended by a random effect term that can be used to account for error induced by the experimental design. The archazolid A treatment was considered as a binary fixed effect whereas biological variations between experiments were taken as a random effect. We allowed the model to fit random intercepts to attribute for variations in the mean values of the control group as well as random interslopes to account for variable differences between the control and the archazolid A-treated group. p values were calculated by a likelihood ratio test.

2.2.16. Western Blot

For analysis of protein levels, Western blot analysis was performed. Firstly, in case of total cell lysates, the cells were lysed using RIPA lysis buffer and freezing cells at -80 °C. In case of subcellular analysis of proteins, cells were fractionated into cytosolic, membrane, mitochondrial and nuclei fraction. Therefore, cells were washed with PBS, 500 µl of buffer A were added and cells were scraped off plates. Subsequently, the lysate was passed through a 25 Ga needle 10x using a 1 ml syringe. After incubation on ice for 20 min, the nuclear pellet was centrifuged out at 720x g for 5 min at 4 °C. The nuclear pellet was washed once with buffer A, resuspended in buffer B and sonicated briefly. The remaining supernatant was centrifuged at 10,000x g, the pellet represents mitochondrial fraction. The supernatant was transferred to ultracentrifugation at 100,000x g for 1 h at 4 °C. The resulting pellet displays the membrane fraction, which was washed once with

buffer A, then dissolved in buffer B and sonicated briefly. The remaining lysate represents the cytosolic fraction.

After protein isolation, the concentrations were determined as bicinchoninic (BC) assay as described previously (61) and measuring the absorbance with SpectraFluor Plus™ plate reader. Briefly, 10 µl protein samples were incubated with 200 µl BC assay reagent (30 min at 37 °C) and absorbance was measured (550 nm). As protein standard a dilution series of bovine serum albumin (BSA) was used and sample protein concentration was determined by linear regression. Equal amounts of protein were loaded onto sodium dodecyl sulfate (SDS)-gels, utilizing Page Ruler™ Prestained as a protein ladder indicator. Proteins were separated by SDS-polyacrylamide gel electrophoresis (SDS-PAGE; 20 min: 100 V, 40 min: 200 V) using the Consort Electrophoresis Power Supply E835 and transferred to nitrocellulose membranes (Amersham Bioscience) by tank blotting (1.5 h: 100 V, 4 °C). To block unspecific antibody binding, membranes were incubated with 5 % blotto for 1 h. Primary antibodies were incubated over night at 4 °C and after washing, secondary antibodies were incubated for 2 h at room temperature. Antibodies were diluted in 5 % BSA (Sigma-Aldrich) in TBST. As secondary antibodies were HRP-coupled ECL substrate was added and chemiluminescence was detected with ChemiDoc Touch Imaging System (Bio-Rad Laboratories GmbH). Quantification of bands was accomplished with Image Lab™ Software (Bio-Rad Laboratories GmbH).

Table 8 Buffers for subcellular fractionation

Buffer A		Buffer B	
Sucrose	250 mM	Sucrose	250 mM
HEPES (pH 7.4)	20 mM	HEPES (pH 7.4)	20 mM
KCl	10 mM	KCl	10 mM
MgCl ₂	1.5 mM	MgCl ₂	1.5 mM
EGTA	1 mM	EGTA	1 mM
EDTA	1 mM	EDTA	1 mM
in H ₂ O		SDS	0.1 %
<i>added before use:</i>		Glycerol	10 %
Complete® EDTA free	4 mM	in H ₂ O	
		<i>added before use:</i>	
		Complete® EDTA free	4 mM

Table 9 Buffers for western blot

RIPA lysis buffer		5x sample buffer	
Tris/HCl (pH 7.4)	50 mM	Tris/HCl (pH 6.8)	3.125 M
NaCl	150 mM	Glycerol	50 %
Nonidet NP-40	1 %	SDS	5 %
Sodium deoxycholate	0.25 %	DTT	2 %
SDS	0.10 %	Pyronin Y	0.025 %
activated Na ₃ VO ₄	0.3 mM	in H ₂ O	
NaF	1 mM		
β-glycerophosphate	3 mM	1x SDS sample buffer	
pyrophosphate	10 mM	5x sample buffer	25 %
in H ₂ O		in H ₂ O	
<i>added before use:</i>			
Complete® EDTA free	4 mM		
PMSF	1 mM		
H ₂ O ₂	0.5 mM		

Table 10 Polyacrylamide gels and electrophoresis buffer

Stacking gel		Separation gel 10 / 12 %	
Rotiphorese™ Gel 30	17 %	Rotiphorese™ Gel 30	33 / 40 %
Tris (pH 6.8)	125 mM	Tris (pH 8.8)	375 mM
SDS	0.1 %	SDS	0.1 %
TEMED	0.2 %	TEMED	0.1 %
APS	0.1 %	APS	0.05 %
in H ₂ O		TCE	0.05 %
		in H ₂ O	
Electrophoresis buffer			
Tris	4.9 mM		
Glycine	38 mM		
SDS	0.1 %		
in H ₂ O			

Table 11 Tank buffers

5x tank buffer		1x tank buffer	
Tris base	240 mM	5x tank buffer	20 %
Glycine	195 mM	Methanol	20 %
in H ₂ O		in H ₂ O	

Table 12 ECL solution

ECL solution	
Tris (pH 8.5)	100 mM
Luminol	2.5 mM
p-Coumaric acid	1 mM
H ₂ O ₂	17 µM
in H ₂ O	

Table 13 Primary Antibodies for Western Blot

Antigen	Company	Cat. No.
ERK 1/2	Cell signaling	9102
pERK 1/2 Thr202/Tyr204	Cell signaling	9106
GAPDH	Santa Cruz	sc-69778
MEK 1/2	Santa Cruz	sc-436
pMEK 1/2 Ser217/221	Cell signaling	9121
panRas	Santa Cruz	sc-14022
Raf 1	Santa Cruz	sc-7267
pRaf-1 Ser 338 / Tyr 341	Santa Cruz	sc-28005-R
PI3K	Upstate	06-195
Akt	Cell Signaling	9272
pAkt (Ser473)	Santa Cruz	sc-7985-R
Bad	Cell signaling	9292
pBad (Ser136)	Cell signaling	9295

Table 14 Secondary Antibodies for Western Blot

Antigen	Company	Cat. No.
Mouse IgG (HRP conjugate)	Santa Cruz	sc-2005
Rabbit IgG (HRP conjugate)	Bio-Rad	172-1019

2.2.17. Ras activity assay

Ras activation status of the cells was determined using the Ras Assay Kit, according to manufacturer's protocol. Cells were seeded 24 h prior to treatment with archazolid (2.5/10 nM, 48 h) and cholesterol (10 µg/ml, 48 h). After stimulation, medium was aspirated off, ice-cold lysis solution, containing GST-Raf-RBD which specifically binds to active GTP-bound Ras, was added and cells were scraped off, using a rubber police man. After centrifugation (12,000x g, 4 °C), supernatant was mixed with Glutathione-Sepharose-Slurry beads, that bind to GST-Raf-RBD and incubated under constant mixing for 30 min at 4 °C. After incubation, beads were spinned down and drained well, mixed with SDS-containing sample buffer for SDS-PAGE, denatured for 10 min at 95 °C and subjected to Western Blot as described in paragraph 2.2.16. Protein loading on the gel was determined using 0.5 % trichloroethanol (Sigma) polyacrylamide gels as described before (62). Primary antibody detecting panRas was provided in the kit and secondary antibody goat-anti-mouse IgG conjugated to HRP were used (Santa Cruz).

2.2.18. Quantitative real-time PCR (qPCR)

Cells were treated as indicated and total mRNA was isolated using the Qiagen RNeasy Mini Kit according to manufacturer's protocol. The concentration of isolated messenger RNA (mRNA) was determined using the NanoDrop® ND-1000 spectrophotometer analyzing the absorption at 260 nm (A260) and 280 nm (A280). The obtained RNA was re-transcribed using the High Capacity cDNA Reverse Transcription Kit according to manufacturer's instructions. Obtained complementary DNA (cDNA) was stored at 4 °C until quantitative real-time Polymerase Chain Reaction (qPCR). The SYBR Green Master Mix was used with the respective primers. Actin served as housekeeping gene. qPCR was performed with the QuantStudio® 3 Real-Time Instrument. Average CT values of target genes were normalized to control as Δ CT. Changes in mRNA expression levels were shown as

fold expression ($2^{-\Delta\Delta CT}$) calculated by the $\Delta\Delta CT$ method normalized to housekeeping gene as described previously (63).

Table 15 Primer sequences used for qPCR

target mRNA	forward sequence	reverse sequence
actin	5' CCA ACC GCG AGA AGA TGA 3'	5' CCA GAG GCG TAC AGG GAT AG 3'
LDL-R	5' CTA CAA GTG GGT CTG CGA TG 3'	5' TTT GCA GGT GAC AGA CAA GC 3'
LX-R	5' TTC ACC TAC AGC AAG GAC GA 3'	5'GAA CTC GAA GAT GGG GTT GA 3'
HMGCR	5' GTC ATT CCA GCC AAG GTT GT 3'	5' GGG ACC ACT TGC TTC CAT TA 3'
SREBP-2	5' ACA AGT CTG GCG TTC TGA GG 3'	5' ACC AGA CTG CCT AGG TCG AT 3'

2.2.19. *In vivo* HUH-7 xenograft mouse model

Thirty-two female SCID mice (Charles River „CB17/lcr-PrkdcSCID/lcrIcocl”) were locally shaved and 3×10^6 HUH-7 cells were injected subcutaneously into the flank of each mouse. Mice were divided into four groups and treated intraperitoneally with 0.2 mg/kg archazolid, 10 mg/kg simvastatin, 0.2 mg/kg archazolid in combination with 10 mg/kg simvastatin in 5 % DMSO / 10 % solutol / PBS or equal amounts of 5 % DMSO / 10 % solutol / PBS. Mice were treated daily. Measurement of tumors was done every 2 to 3 days with a caliper, using the formula $a \times b^2/2$. The average tumor volumes of the two groups were compared over time. *In vivo* experiments were executed by Melanie Ulrich and Kerstin Loske (Group of Prof. Dr. Angelika M. Vollmar, University of Munich, Pharmaceutical Biology). Animal experiments were approved by the District Government of Upper Bavaria in accordance with the German animal welfare and institutional guidelines.

2.2.20. Immune histochemistry (IHC)

IHC analysis of tumor tissue sections was performed as described previously [49] using anti-LAMP1-antibody (Abcam), filipin (Sigma Aldrich), anti-Ki67-antibody and haematoxylin (Sigma Aldrich).

For Ki67 staining, paraffin embedded tumor sections were de-paraffinated by incubation in xylol, followed by ethanol 100 %, ethanol 95 % and water. For antigen retrieval, tissue sections were incubated in sodium citrate buffer at 95 °C for 20 min. After cooling, sections were washed two times with 0.05 % triton-X in PBS, peroxidase activity was quenched with 7.5 % H₂O₂ in water for 10 min at room temperature and unspecific binding was blocked with blocking serum of the VECTASTAIN Elite ABC HRP Kit for 20 min at room temperature. Sections were incubated with anti-Ki67-antibody (ab-15580, abcam) for 1 h at room temperature, washed twice with PBS, incubated with secondary antibodies and universal reagent of the VECTASTAIN Elite ABC HRP Kit. After washing, AEC substrate from the ImmPACT AEC Peroxidase (HRP) Substrate kit was added for 30 min. After additional washing, haematoxylin counterstaining was performed, sections were washed and mounted in FluorSafe™ and sealed with cover slides. Ki67 staining was evaluated using the Olympus BX41 microscope.

For LAMP-1 and cholesterol staining the same procedure was used, however, secondary antibody mouse IgG (AlexaFluor 488 conjugate) and filipin were added in blocking solution of the VECTASTAIN elite ABC HRP Kit for 2 h at room temperature. Cholesterol and LAMP-1 staining were evaluated by confocal microscopy using a Leica TCS SP 8 SMD confocal microscope.

Table 16 Buffer for IHC

Sodium citrate buffer	
Tri-Na-Citrate(dihydrate)	10 mM
Tween	0.5 %
HCl	ad pH 6.0
in H ₂ O	

2.2.21. Statistical Analysis

All experiments were performed at least three times unless stated otherwise. Statistical analysis was performed using GraphPad Prism® (GraphPad Software, Inc., La Jolla, CA, USA). Graph data represent means ± SEM. One-way ANOVA/Dunnett's multiple comparison test and individual unpaired t-tests were conducted. p values less than 0.05 were considered significant.

RESULTS

3. RESULTS

3.1. V-ATPase inhibition induces cancer cell stiffening and alters membrane fluidity in HCC

3.1.1. Real-time deformability cytometry reveals cancer cell stiffening due to V-ATPase inhibition

Biophysical characteristics of cancer cells have come into focus lately, regarding the search for new therapy options. In this context, it has been reported that increased softness of cancer cells correlates with malignancy (46). Interestingly, the V-ATPase has been reported to regulate cholesterol metabolism (10,11,23), a fact which lead to the working hypothesis that inhibition of V-ATPase by archazolid A might influence cancer cell biophysical properties. To elucidate this hypothesis, we utilized a relatively new method to analyze the deformation of cells, the real-time deformability cytometry (RT-DC) in collaboration with Dr. Maria Winzi (Group of Prof. Dr. Jochen Guck, Biotec, TU Dresden). RT-DC is a microfluidic-based technique which allows the measurement of cell deformation while cells pass through a narrow constriction with a rate of 100 cells/s (59).

We analyzed the influence of archazolid A treatment on the deformability of HUH-7 cancer cells and the non-malignant hepatocyte-like cell line HepaRG. Firstly, we assessed the influence of the applied flow rates on the deformation, as they correlate with shear force subjected to the cells. We found that at all applied flow rates, HUH-7 cells behaved similarly (Fig 14 A). In general, we could show that HUH-7 control cells change their shape to a rather oval structure, whereas treated HUH-7 cells remain quite spherical (Fig 14 C). Secondly, we also monitored the behavior of HepaRG cells at different flow rates and revealed that also for the non-malignant cells, effects are independently of the force applied (Fig 14 B). To exclude that cellular shape is altered directly by stimulation, cells were imaged in the reservoir before entering the channel, however, no difference was detected (Fig 14 A, B). Taken together, the RT-DC measurements clearly showed that treatment reduces overall deformability of HUH-7 cells (Fig 14 D), whereas deformability of HepaRG remained unaffected (Fig 14 E), indicating a cancer cell selectivity of the effect.

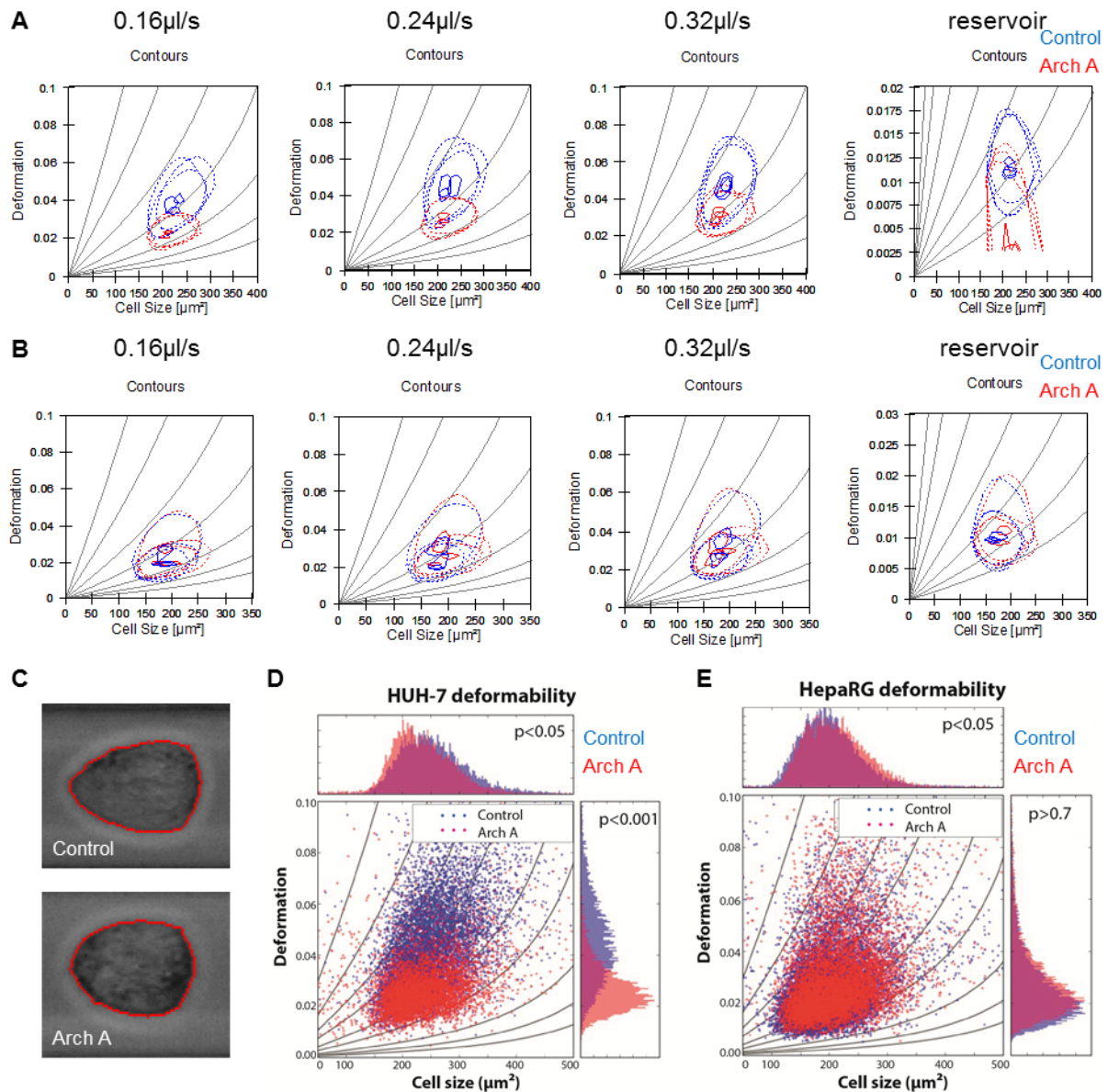


Figure 14 V-ATPase inhibition selectively reduces deformability of cancer cells in RT-DC measurements HUH-7 (**A**) and HepaRG (**B**) cells were left untreated (blue) or were treated with archazolid A (10 nM, 24 h) (red) and subjected to flow rates of 0.16 μ l/s, 0.24 μ l/s or 0.32 μ l/s or no shear stress (reservoir). Blots show contours of dot blots of deformation compared to cell size. (**C**) Representative images of an HUH-7 control cell (upper image) and an archazolid A (10 nM, 24 h) treated cell (lower image) when subjected to shear force in the flow channel (0.24 μ l/s). Red line indicates outline for calculation of deformation. (**D, E**) Representative dot blots of deformation compared to cell size at a flow rate of 0.16 μ l/s for HUH-7 and HepaRG, respectively. Blue dots represent control cells, red dots represent archazolid A treatment (10 nM, 24 h). Graphs represent cell size (cross sectional area) versus deformation (1-circularity) with isoelasticity lines representing areas of identical stiffness. $p^* < 0.01$, p -values of three independent experiments with > 3000 cells per experiment were determined by a likelihood ratio test.

3.1.2. V-ATPase inhibition induced cell stiffening due to alterations in membrane properties

The stiffness of cells in general is mainly influenced by two factors: the cytoskeleton and the membrane. As we could detect no evident differences in actin cytoskeleton of HUH-7 cells (Fig 15), we focused on possible effects of archazolid A treatment on the membrane.

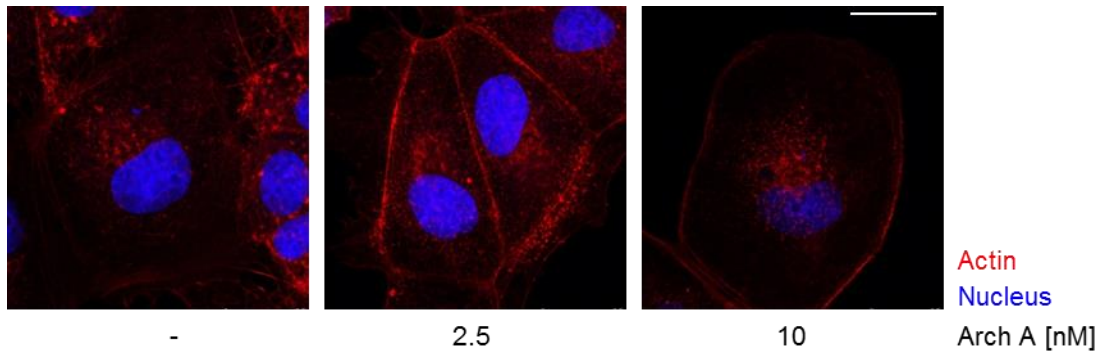


Figure 15 V-ATPase inhibition shows no evident influence on actin cytoskeleton HUH-7 cells were treated with archazolid A as indicated (24 h) stained for actin (red) and nuclei (blue) and analyzed by confocal microscopy. Representative images out of three independent experiments are shown. Scale bar 25 μm .

For this purpose, we analyzed plasma membrane fluidity, using a fluorescence-recovery after photo-bleaching (FRAP) approach on cells transfected with a membrane-targeted (i.e. farnesylated) GFP coding plasmid. After bleaching fluorescence in a specific membrane area, recovery was monitored over time and the speed constant was calculated as described in the methods section (2.2.10). In control cells, the bleached area was repaired relatively fast, whereas in archazolid A treated cells the restoration of fluorescence was hindered (Fig 16 A). Hence, the recovery constant was significantly slower in treated cells compared to control cells (Fig 16 B). This finding indicates reduced lateral mobility of farnesylated proteins in the plasma membrane of archazolid A treated cells.

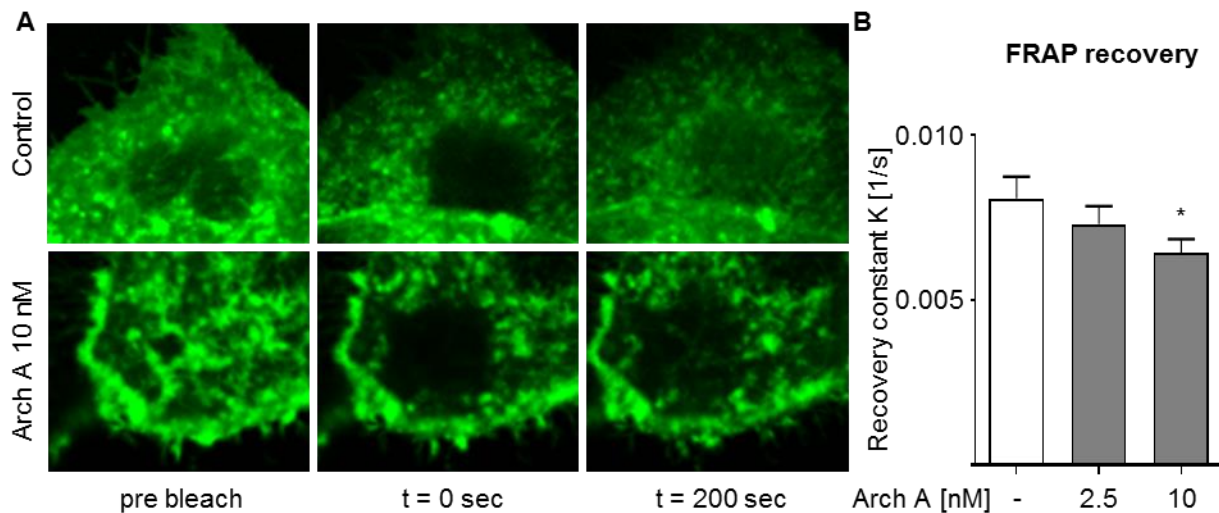


Figure 16 V-ATPase inhibition causes alterations in membrane fluidity (A, B) FRAP of HUH-7 cells transfected with membrane targeted (farnesylated) GFP and treated with archazolid A (10 nM, 24 h) was analyzed by confocal microscopy. Recovery speed constant K was calculated by non-linear curve fit. One representative image and diagram of FRAP recovery of three independent experiments are shown. Bars are the mean \pm SEM of three independent experiments. $p^* < 0.05$ One-way ANOVA, Dunnett post test

The plasma membrane of mammalian cells is composed of a variety of different lipids and proteins, which influence membrane biophysical properties, localization of signaling molecules and fluidity (64). In order to investigate the cause of the reduced lateral mobility of farnesylated proteins, we investigated specifically polarity of the membrane. Therefore, we used the membrane-intercalating, polarity sensitive dye di-4-ANEPPDHQ. This dye undergoes a 60 nm spectral blue shift between disordered and ordered membrane compartments, representing non-raft and cholesterol-rich lipid-raft membrane regions, respectively. These special fluorescent properties of di-4-ANEPPDHQ allow a quantitative analysis of membrane polarity, by calculating a value for generalized polarization (GP), as described previously (65).

Treatment with archazolid A resulted in a drop of GP values, indicating an increase in membrane polarity in HUH-7 and HepG2 cells. In contrast, the non-malignant HepaRG cells and primary human hepatocytes (hHep) showed no change in membrane polarity following treatment. (Fig 17 A). For easy visualization, heat map images (Fig. 17 C) and GP value distribution histograms (Fig. 17 D) were compiled. To exclude responsibility of an off-target event for increased membrane polarity, we performed siRNA mediated knock-down of the V-ATPase and subsequently

measured GP values. Knocking-down V-ATPase also reduced GP values, confirming V-ATPase dependency of the mechanism (Fig 17 B). These results clearly depict the ability of archazolid A to alter biophysical characteristics selectively in cancer cells, while leaving non-malignant cells unaffected.

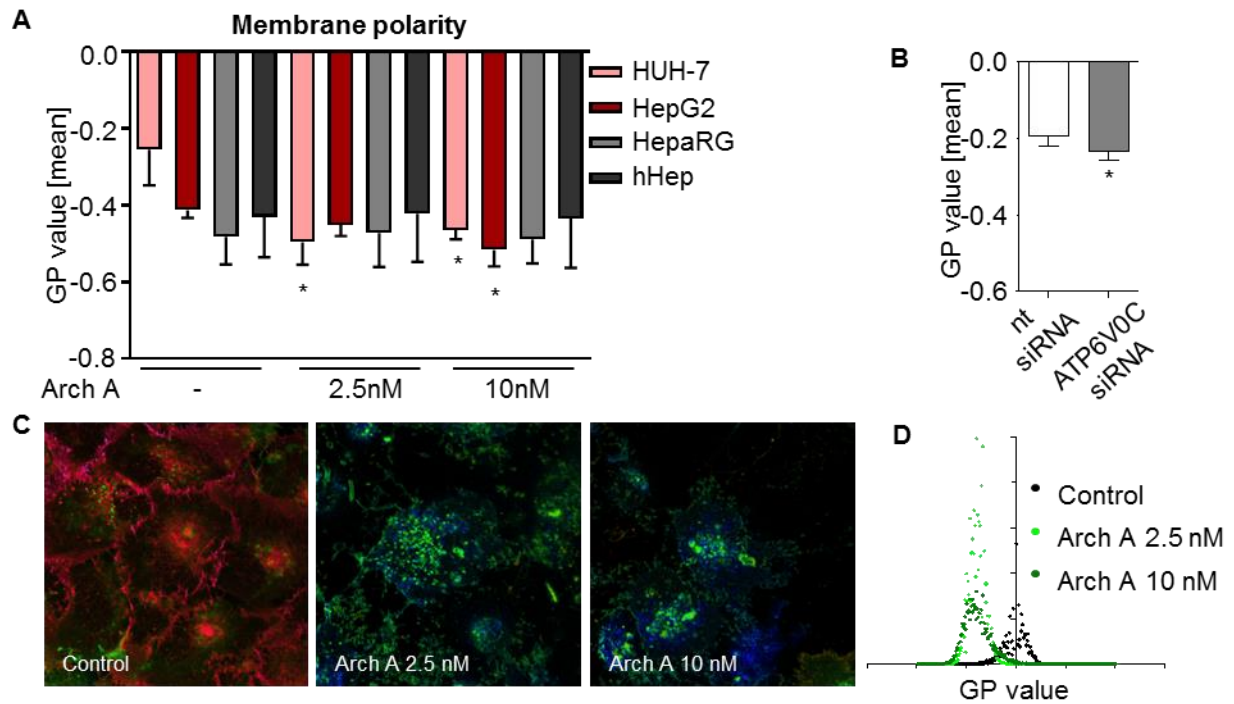


Figure 17 V-ATPase inhibition leads to an alteration in plasma membrane composition (A) HUH-7, HepG2, HepaRG and hHep were treated with archazolid A as indicated (2.5/10 nM, 24 h) and (B) HUH-7 cells were transiently transfected with nt siRNA or siRNA silencing c-subunit of the V-ATPase (ATP6V0C siRNA) (72 h). Membrane polarity was analyzed by confocal microscopy of live cells stained with di-4-ANEPPDHQ. Representative heat map images (C) and histogram (D) of generalized polarization (GP) value distribution of HUH-7 di-4-ANEPPDHQ stainings are shown. A GP value drop indicates increased membrane polarity. Bars are the mean \pm SEM of three independent experiments. $p^* < 0.05$ One-way ANOVA, Dunnett post test (A) or unpaired t-test (B)

3.2. V-ATPase inhibition alters cholesterol metabolism of HCC cells

We could show that archazolid A alters plasma membrane properties of cancer cells. The plasma membrane of eukaryotic cells is composed of phospholipids, sphingolipids and the rather unipolar sterol cholesterol (66). In order to determine the cause for reduced fluidity and increased membrane polarity, we focused on analyzing membrane components.

3.2.1. Availability of free cholesterol is diminished upon V-ATPase inhibition

We focused on cholesterol metabolism, as it has been reported recently to be influenced by the V-ATPase (10). Employing the enzyme-based Amplex Red® cholesterol measurement kit, we evaluated levels of both, total and free cholesterol. The assay revealed, that treatment with archazolid A led to a reduction in the proportion of free cholesterol in HCC cell lines, yet leaving non-malignant cells unaffected (Fig 18 A). In HUH-7 cells, knock-down of the V-ATPase also reduced the proportion of free cholesterol within the cell, ensuring a V-ATPase dependent mechanism (Fig 18 B).

Additionally, we conducted ultraperformance liquid chromatography-coupled ESI tandem mass spectrometry (UPLC-MS/MS) measurements in cooperation with Dr. Andreas Koeberle (Group of Prof. Oliver Werz, Institute of Pharmacy, Friedrich Schiller University Jena). UPLC-MS/MS analysis of cholesteryl-ester (CE) species in archazolid A treated HUH-7 cells showed, that while the overall amount of CE within the cells is not altered (Fig 18 C), the composition of CE changes upon V-ATPase inhibition (Fig 18 D). These data point to a role of V-ATPase in the availability of free cholesterol and CE composition.

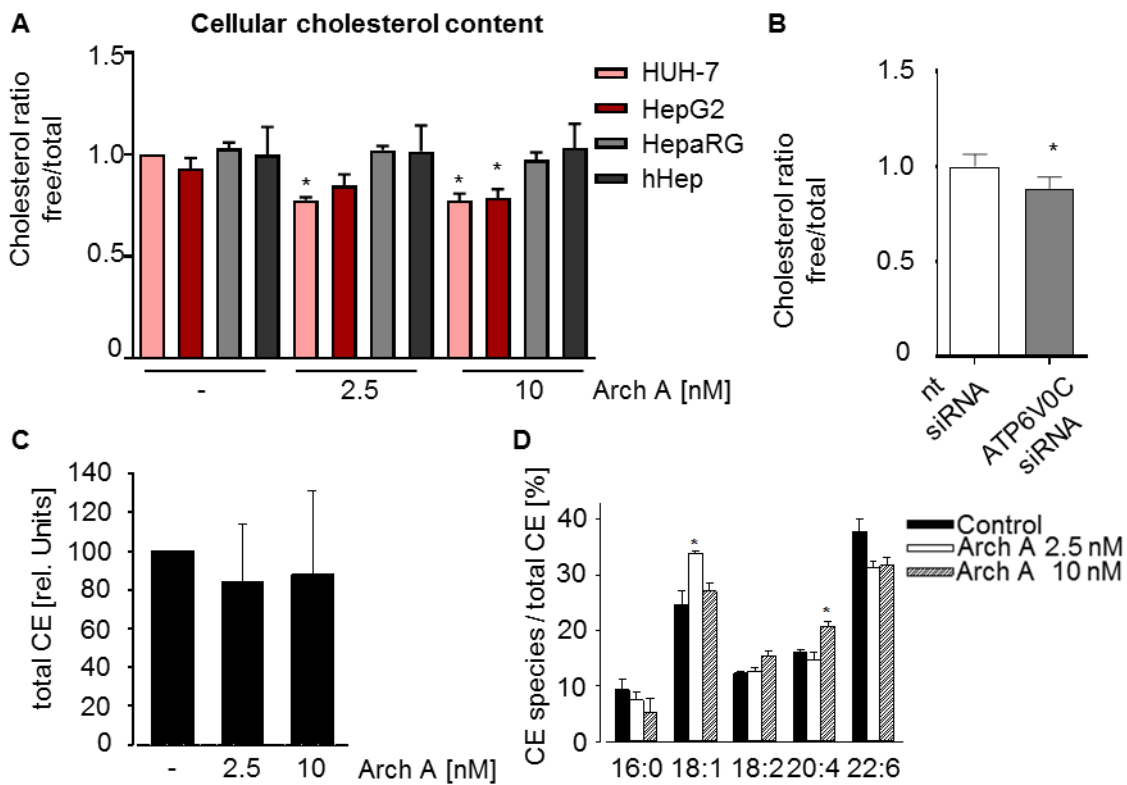


Figure 18 V-ATPase inhibition reduces free cholesterol levels and alters cholesteryl-ester composition (A) Ratio of levels of free to total cholesterol of HUH-7, HepG2, HepaRG and hHep cells treated with archazolid A (2.5/10 nM, 48 h) assessed by Amplex Red® assay. **(B)** HUH-7 cells were transiently transfected with nt siRNA or siRNA silencing c-subunit of the V-ATPase (ATP6V0C siRNA) (72 h) and cholesterol content was analyzed. **(C, D)** HUH-7 cells were treated with archazolid A (2.5/10 nM, 48 h), lipids were extracted and CE composition was analyzed by mass spectrometry. Bars are the mean \pm SEM of three independent experiments. $p^* < 0.05$ One-way ANOVA, Dunnett post test **(A, C, D)** or unpaired t-test **(B)**

3.2.2. V-ATPase inhibition impedes internalization of LDL via the LDLR and enhances LDLR expression

Free cholesterol availability in mammalian cells is dependent on supply by *de novo* synthesis or by uptake of cholesterol as main component of low-density lipoprotein (LDL) via its respective receptor (LDLR), however uptake by internalization is the primary cholesterol source. In previous studies of our group, we showed an inhibition of EGF and transferrin receptor recycling by archazolid (11,23), hence we hypothesized a similar fate for the LDLR.

Therefore, we analyzed the presence of the LDLR on the surface of HUH-7 cells. Flow cytometry with labelled antibody conjugates revealed an increased amount of the LDLR on the surface of archazolid A treated HUH-7 cells (Fig 19 A). Enhanced

surface appearance can be caused by several ways in principle, on the one hand by increased expression of the protein and on the other hand by reduced internalization. In order to investigate the underlying mechanism we analyzed LDLR expression level upon archazolid A treatment by quantitative real-time PCR (qPCR). The experiment revealed increased expression of the receptor on mRNA level upon inhibition of the V-ATPase (Fig 19 B).

So as to investigate the effect of archazolid A on LDLR internalization, we used two different strategies. Firstly, we performed an LDLR internalization assay with a fluorescently labelled antibody conjugate (Fig 19 C). After internalization, LDLR distribution within the cell was visualized by confocal microscopy. In control cells, LDLR is properly internalized, leading to intracellular bright green dots in the confocal image (Fig 19 C, upper lane). Following archazolid A treatment, the green signal disappears leaving only diffuse membrane staining (Fig 19 C, lower lane), pointing to a reduction in internalization. In a second approach, we used a labelled LDL conjugate (Fig 19 D). In a similar internalization assay, we could show that LDL is properly internalized in control cells (Fig 19 D, upper lane), but internalization is diminished by archazolid A treatment, leading to accumulation of LDL at the outer boarder of the cells (Fig 19 D, lower panel).

Taken together, these findings clearly show that treatment with archazolid A leads to increased LDLR transcription and a decreased LDLR internalization, followed by a decreased uptake of LDL together with an increased presence of LDLR on the cellular surface, thereby most likely disturbing cholesterol metabolism.

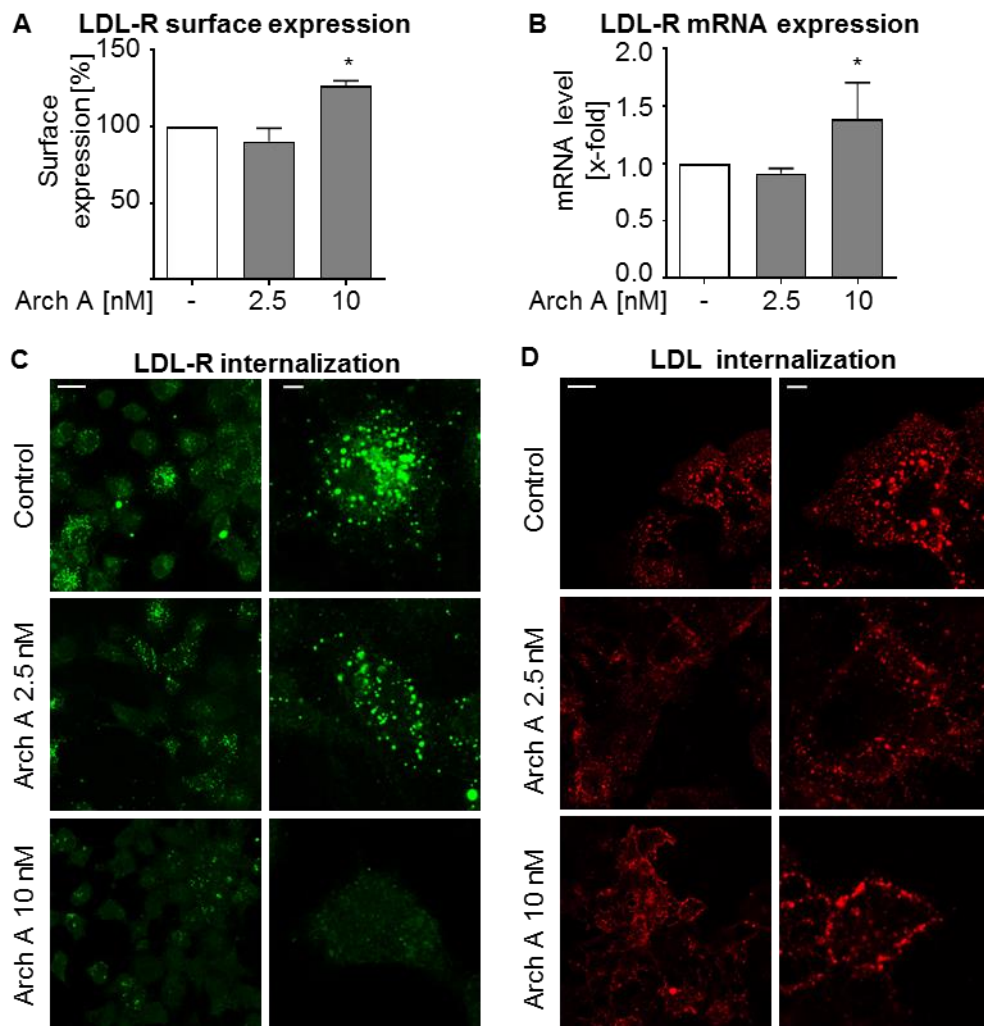


Figure 19 LDLR internalization and LDL uptake is inhibited by archazolid A treatment (A) LDLR surface expression of HUH-7 cells was visualized by antibody staining and analyzed by flow cytometry after archazolid A treatment (2.5/10 nM, 24 h). (B) Relative mRNA expression levels of LDLR in HUH-7 cells were detected with the AB 7300 RealTime PCR system. Bars are the mean \pm SEM of three independent experiments. $p^* < 0.05$ Repeated measures ANOVA, Dunnett post test (C) HUH-7 cells were treated with archazolid A (2.5/10 nM, 24 h) and subsequently starved for 2 h. After incubation with PMA (1 h) internalized LDLR was visualized by antibody staining and analyzed by confocal microscopy. (D) HUH-7 cells were treated with archazolid A (2.5/10 nM, 24 h) and subsequently starved for 1.5 h. Internalization of DiILDL (fluorescently labeled soluble LDL) was analyzed by confocal microscopy. Representative images out of three independent experiments are shown. Scale bar 25 μ m (left columns) and 5 μ m (right columns), respectively.

3.2.3. V-ATPase inhibition leads to cholesterol trapping and induction of *de novo* synthesis

In summary, our previous data show a restriction of free cholesterol, plasma membrane cholesterol depletion and a reduction of LDL uptake, however, the question where the free cholesterol is located still remained. In order to clarify this issue, we investigated subcellular localization of cholesterol. As free cholesterol is mainly released from lysosomes under normal conditions and lysosomes greatly depend on a functional V-ATPase, we assumed lysosomes as location for the restricted cholesterol in archazolid A treated cells.

We hence isolated lysosomes from treated cells as described previously (56), and measured cholesterol levels employing the Amplex Red® cholesterol measurement kit. The analysis showed, that the amount of cholesterol in purified lysosomes drastically increases due to archazolid A treatment (Fig 20 A). This finding could further be supported by a confocal staining for cholesterol and the lysosomal marker protein LAMP-1. Control cells displayed a fine dispersion of LAMP-1 and cholesterol within the cell, whereas archazolid A treated cells showed huge accumulations of colocalized stainings (Fig 20 B), indicating a cholesterol trapping within the lysosomes of treated cells.

Since archazolid A treated cells obviously suffer from cholesterol depletion, due to trapping in the lysosomes and impaired uptake, we supposed that the cells might upregulate *de novo* cholesterol synthesis. We therefore investigated the impact on cholesterol regulating genes SREBP-2 and HMGCR of archazolid A single treatment and combination treatment of archazolid A with the cholesterol synthesis inhibitor simvastatin to block possibly increased synthesis. qPCR analysis showed, that cells indeed upregulate the expression of SREBP-2 (Fig 20 C), the master regulator of cholesterol synthesis and also the expression of HMGCR (Fig 20 D). HMGCR is the direct target of simvastatin and catalyzes the reduction of HMG-CoA to mevalonate, the rate-limiting step of cholesterol synthesis. As expected, combination therapy further enhanced archazolid A induced upregulation of transcription, indicating a feedback regulation, due to cholesterol depletion.

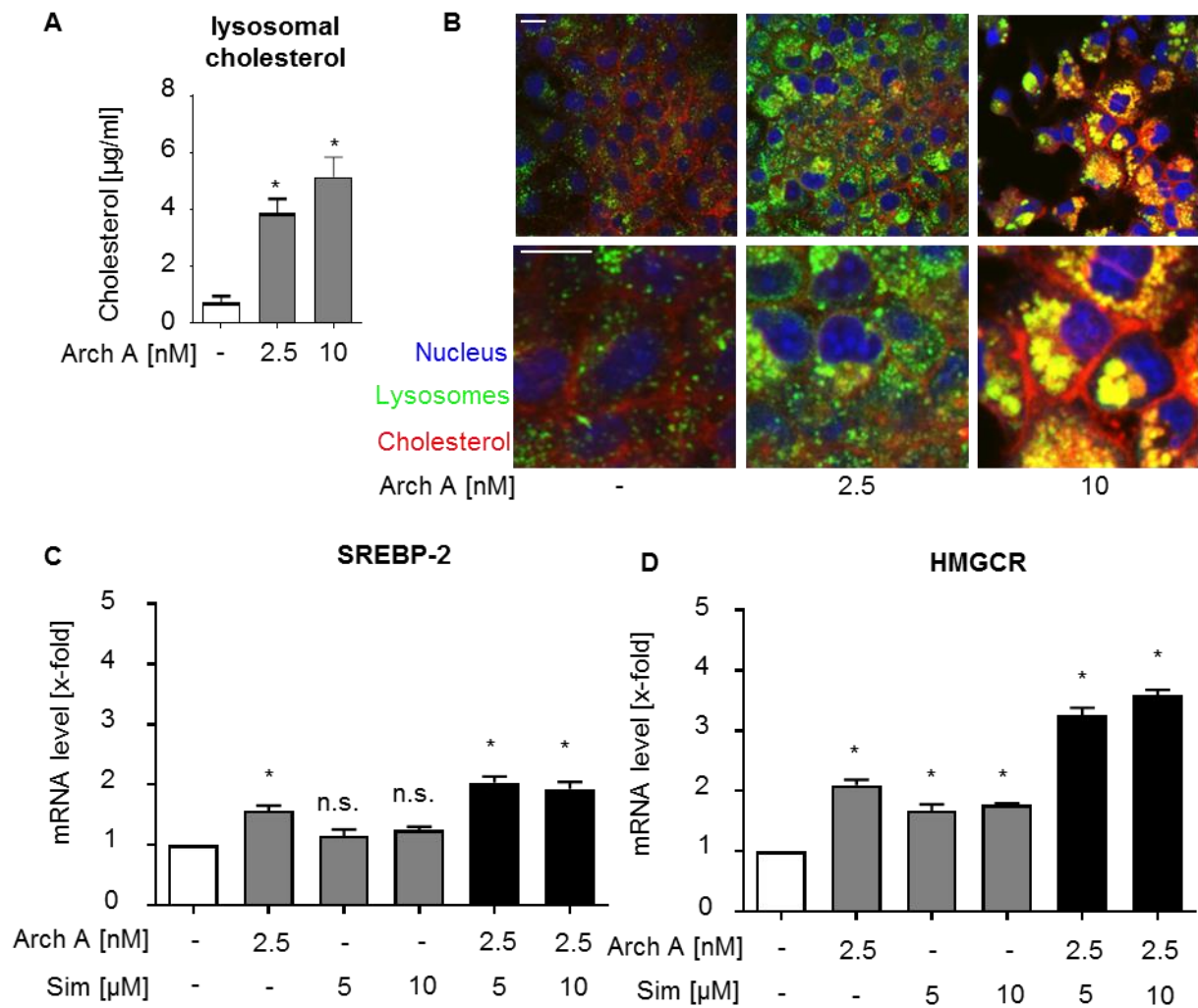


Figure 20 Lysosomal cholesterol trapping and induction of *de novo* cholesterol synthesis due to archazolid A treatment (A) HUH-7 cells were treated with archazolid A as indicated (2.5/10 nM, 48 h) and lysosomes were isolated. Levels of total cholesterol in lysosomes were analyzed by AmplexRed® assay. **(B)** HUH-7 cells were treated as indicated (2.5/10 nM, 24 h), stained for cholesterol (red), lysosomes (green) and nuclei (blue) and analyzed by confocal microscopy. Representative images out of three independent experiments are shown. Scale bar 20 µm. **(C, D)** HUH-7 cells were treated as indicated with archazolid A, simvastatin or a combination of both compounds as indicated for 24 h. Relative mRNA expression levels of SREBP-2 and HMGCR respectively, were detected with the AB 7300 RealTime PCR system. Bars are the mean ± SEM of three independent experiments. $p^* < 0.05$ Repeated measures ANOVA, Dunnett post test

3.3. Plasma membrane cholesterol depletion leads to impaired Ras signaling

3.3.1. Activation of the small GTPase Ras is impaired upon V-ATPase inhibition

As cholesterol homeostasis is disrupted due to lysosomal trapping leading to plasma membrane cholesterol depletion, we were interested in possible functional consequences. Cholesterol-rich lipid-rafts are particularly important signaling platforms for the activation of farnesylated proteins (52), so we investigated the impact of archazolid A treatment on the small GTPase Ras. First of all, we checked for changes in the overall protein level of Ras, yet could not determine any changes following treatment (Fig 21 A). In a second approach, we performed a subcellular fractionation to obtain the membrane fraction of the cells, in which we quantified Ras protein expression. We could observe a significant reduction of Ras protein levels within membrane fractions (Fig 21 B) and furthermore, confocal staining of Ras showed that while the signal is finely dispersed over the whole cell in control cells, the Ras staining is restricted to few accumulations in archazolid A treated cells (Fig 21 C). These findings point to a mislocalized Ras protein, leading to the assumption that Ras activation might be hindered.

To test this hypothesis, we precipitated active Ras in whole cell lysates of treated and control cells and found that the amount is decreased upon archazolid A treatment (Fig 21 D). To proof that inhibition of Ras activation is cancer cell specific, we induced Ras signaling in the non-malignant HepaRG cells by EGF treatment and then observed the effect of archazolid A on active Ras. The fact that we could not observe changes in active Ras levels in HepaRG cells (Fig 21 E) indeed points to a tumor specific effect. To verify plasma membrane cholesterol depletion as underlying mechanism of decreased Ras activation, we added soluble cholesterol to the medium of treated cells and quantified Ras activation. Ras remained active despite archazolid A treatment when medium was supplemented with cholesterol (Fig. 21 F) confirming a cholesterol dependency.

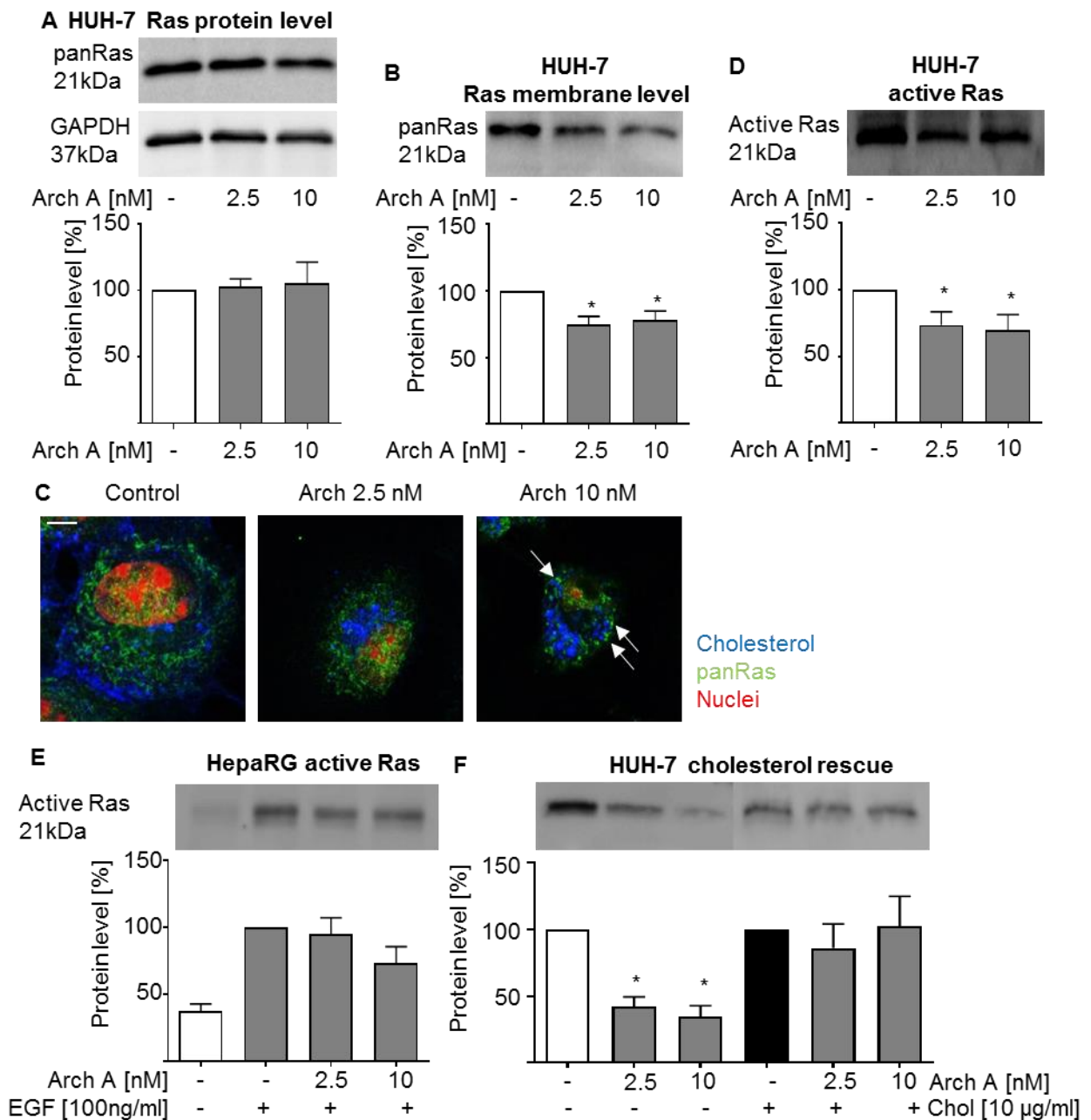


Figure 21 Archazolid A reduces Ras activation in a cholesterol-dependent manner (A) PanRas protein expression of HUH-7 cells was detected by western blot (WB) upon archazolid A treatment (48 h). **(B)** PanRas protein level in membrane fractions of archazolid A (48 h) treated HUH-7 was detected by WB. **(C)** HUH-7 cells were treated as indicated (2.5/10 nM, 24 h), stained for cholesterol (blue), panRas (green) and nuclei (red) and analyzed by confocal microscopy. White arrow heads show Ras accumulations. Representative images out of three independent experiments are shown. Scale bar 20 µm. **(D, E)** Active Ras was precipitated in cell lysates of archazolid A treated (48 h) HUH-7 and HepaRG cell lysates and analyzed by WB, respectively. In HepaRG cells Ras signaling was stimulated by EGF (100 ng/ml) treatment 15 min prior to lysis. **(F)** HUH-7 cells were treated with archazolid A together with or without cholesterol as indicated (48 h). Active Ras was precipitated in cell lysates and detected by WB. Bars are the mean ± SEM of three independent experiments. $p^* < 0.05$ One-way ANOVA, Dunnett post test

3.3.2. Ras downstream signaling is altered upon treatment

Signaling of the small GTPase Ras is of crucial importance for various downstream signaling pathways within the cell. Most prominent are the MAPK pathway and the PI3K/Akt pathway (52). In order to examine possible effects on downstream signaling, we performed western blot experiment on various different downstream regulators.

Our data show that the activating phosphorylation of Raf-1, MEK 1/2 and ERK 1/2 is reduced upon archazolid A treatment (Fig 22 A), indicating an inhibition of the MAPK pathway, whereas PI3K/Akt remains unaffected (Fig 22 B). To compensate a possible escape mechanism by increased cholesterol synthesis, we additionally treated cells with simvastatin. Simvastatin treatment alone did not affect MAPK or PI3K/Akt signaling and combination therapy showed similar effects as archazolid A single treatment (Fig 22 A, B).

In these experiments we could show that archazolid A reduces MAPK signaling downstream of Ras activation.

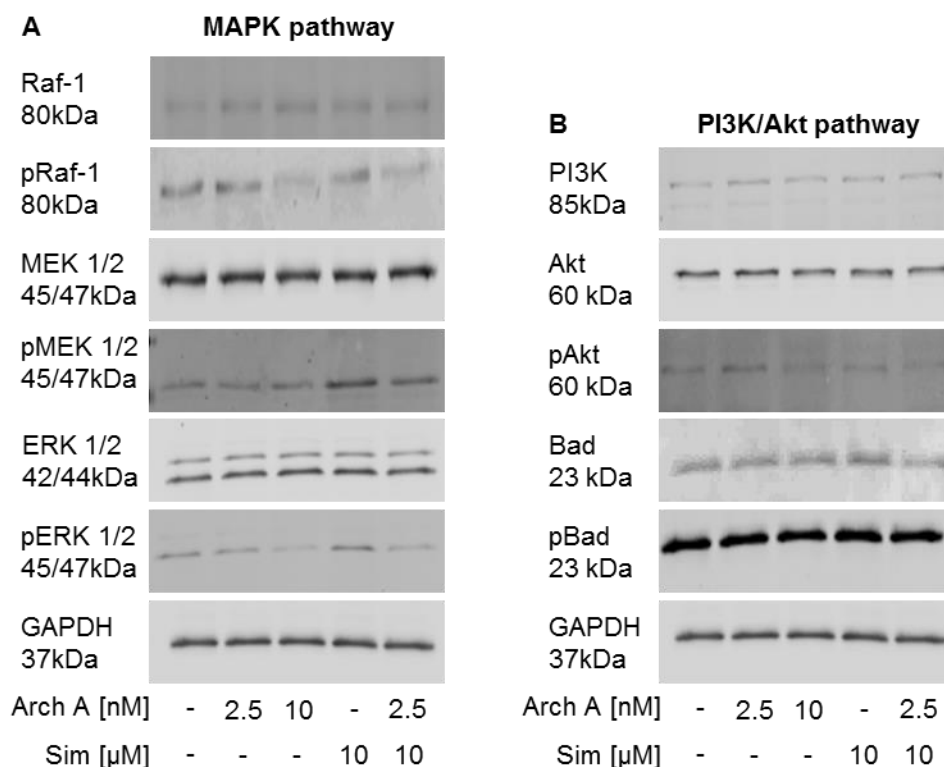


Figure 22 Effect of archazolid A on Ras downstream signaling Protein expression of Raf-1, pRaf-1 (Ser338/Tyr341), MEK 1/2, pMEK 1/2 (Ser217/221), ERK 1/2 and pERK 1/2 (Thr202/Tyr204) (**A**) or PI3K, Akt, pAkt (Ser473), Bad and pBad (Ser136) (**B**) of HUH-7 cells treated with archazolid A, simvastatin or combination (48 h) was analyzed by WB. GAPDH served as loading control.

3.4. A combination therapy approach to inhibit HCC proliferation

3.4.1. A combination of archazolid and simvastatin leads to synergistic growth inhibition of HCC cells *in vitro*

We showed that archazolid A is able to restrict cholesterol access and to cause inhibition in MAPK signaling due to cholesterol depletion in a Ras dependent manner. As Ras signaling is essential for cancer cell proliferation we investigated the influence of archazolid A in a CellTiter Blue proliferation assay. Treatment of the cancer cell lines HUH-7 and HepG2 resulted in a strong, concentration dependent inhibition of proliferation, while HepaRG cells remained unaffected (Fig 23 A) supporting the previously detected cancer cell specificity.

As we had observed an upregulation of cholesterol synthesis regulating genes SREBP-2 and HMGCR (see Fig 20 C, D), we assumed that a combination therapy of archazolid A with the HMGCR inhibitor simvastatin might be beneficial for treatment, despite the fact that simvastatin treatment did not significantly affect Ras downstream signaling (see Fig 21 A, B). Firstly, we analyzed the ability of simvastatin single treatment on the proliferation of HCC cells. A CellTiter Blue assay revealed that simvastatin single treatment concentration dependently reduced the ability of HCC cells to proliferate (Fig 23 B). In a second approach we investigated the beneficial effect on proliferation of a combination therapy with both drugs. We could show that the combination therapy synergistically inhibits proliferation of HUH-7 and HepG2 cells *in vitro* (Fig 23 C).

The MAPK pathway is known to be important in the regulation of proliferation. However, induction of apoptosis might also be responsible for the reduced viability of HCC cells in the CTB assay. To address this question, we determined apoptosis and found that apoptosis is almost at control level in single treatment and only mildly increased in combination therapy (Fig 23 D), indicating inhibition of proliferation as main mechanism of action. In addition, we could show that combination therapy also has a long-term inhibiting effect on proliferation, as determined by clonogenic survival assay (Fig 23 E).

In conclusion, our data show a strong anti-proliferative effect of archazolid A on HCC cells and a clearly beneficial effect of combining archazolid A with simvastatin *in vitro*.

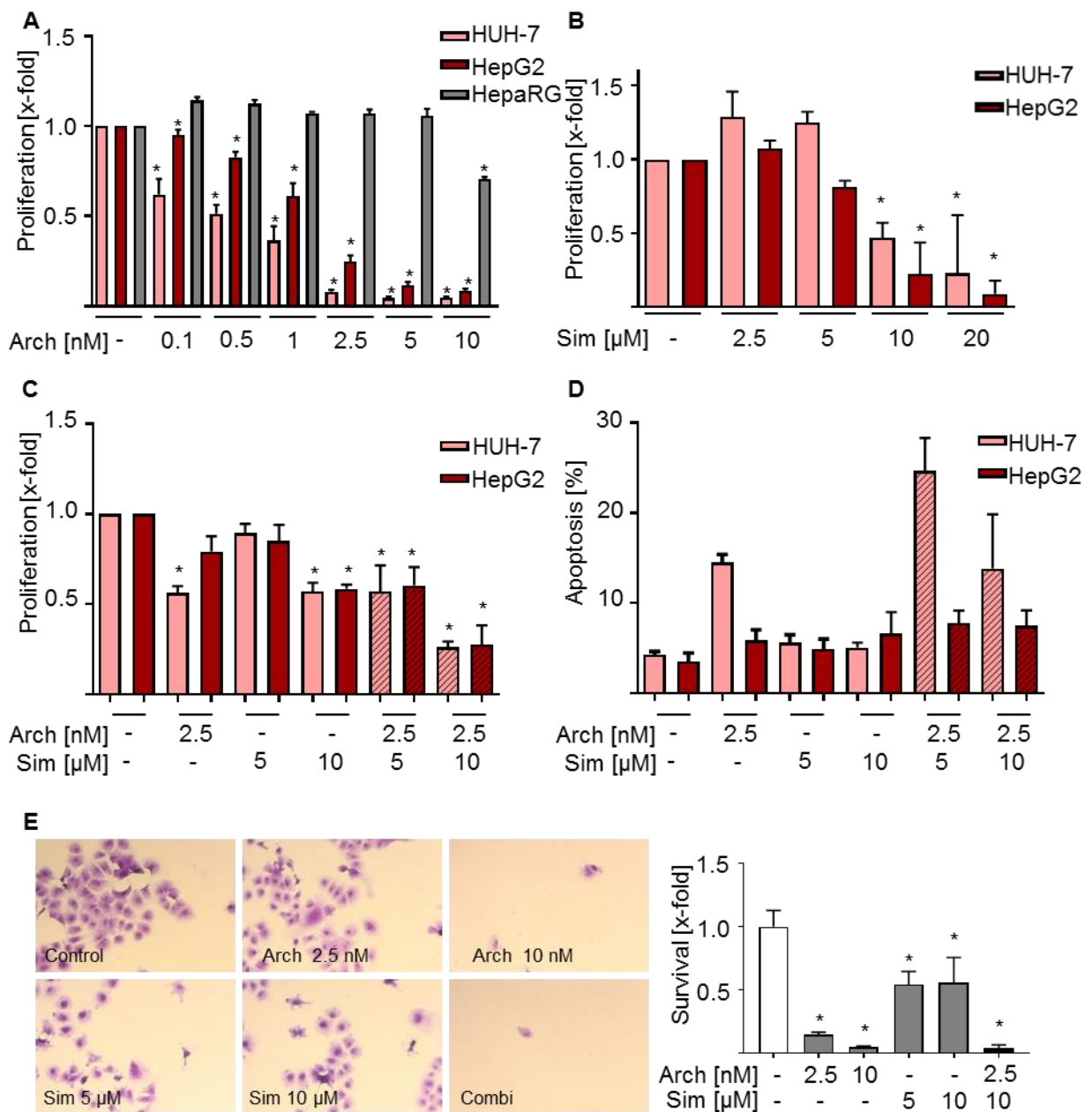


Figure 23 Combination therapy with archazolid A and simvastatin shows strong anti-proliferative effects (A) Proliferation of HUH-7, HepG2 and HepaRG cells was analyzed in a CellTiter Blue assay, after treatment as indicated with archazolid A (72 h). **(B, C)** Proliferation of HUH-7 and HepG2 was analyzed in a CellTiter Blue assay after treatment with simvastatin or combination therapy as indicated (72 h), respectively. **(D)** Apoptotic cell death of HUH-7 and HepG2 cells treated as indicated (48 h) was analyzed by PI staining and subsequent flow cytometry. **(E)** HUH-7 cells were pre-treated as indicated for 24 h and subjected to clonogenic survival for 7 d. Colonies were stained with crystal violet and imaged at 10x magnification. Crystal violet was re-dissolved and staining was assessed by measurement of absorption. Bars are the mean \pm SEM of quantification of three independent experiments. $p^* < 0.05$ One-way ANOVA, Dunnett post test

3.4.2. Archazolid strongly inhibits tumor growth in an *in vivo* mouse xenograft model

Following the quite promising effects of a combination therapy on *in vitro* proliferation, we performed a HUH-7 mouse xenograft model. Importantly, daily treatment of mice bearing solid tumors with archazolid for 10 days resulted in a significant decrease in tumor size at study endpoint (Fig 24 A, red bar). Also the respective growth rate of tumors in archazolid treated mice was significantly slower than in control group (Fig 24 B, red curve). Surprisingly, treatment of mice with simvastatin lead to slightly increased tumor volume at study end point (Fig 24 A, yellow bar) and an increased proliferation rate (Fig 24 B, yellow curve). This resulted in a tumor volume comparable to control cells, and only a slightly reduced proliferation rate of tumors in animals treated with a combination therapy (Fig A and B, orange bar and curve).

Since the liver is the primary organ in regulating cholesterol homeostasis *in vivo*, livers were dissected at study endpoint to check for obvious side effects of treatment. Visual examination of the livers showed no obvious signs for severe side effects like e.g. fatty livers (Fig 24 C).

Consistent with the reduction in proliferation rate and reduced tumor volume upon archazolid treatment, expression of the proliferation marker Ki67 was significantly reduced in tissue samples of tumor sections (Fig 24 D). Furthermore, staining of tumor sections for cholesterol and lysosomes revealed lysosomal accumulation as expected by our *in vitro* data.

Taken together, we could show that archazolid strongly inhibits proliferation of HCC cells *in vitro* and *in vivo* by cholesterol restriction to the lysosomes. However, a combination therapy of archazolid and simvastatin *in vivo* needs further evaluation.

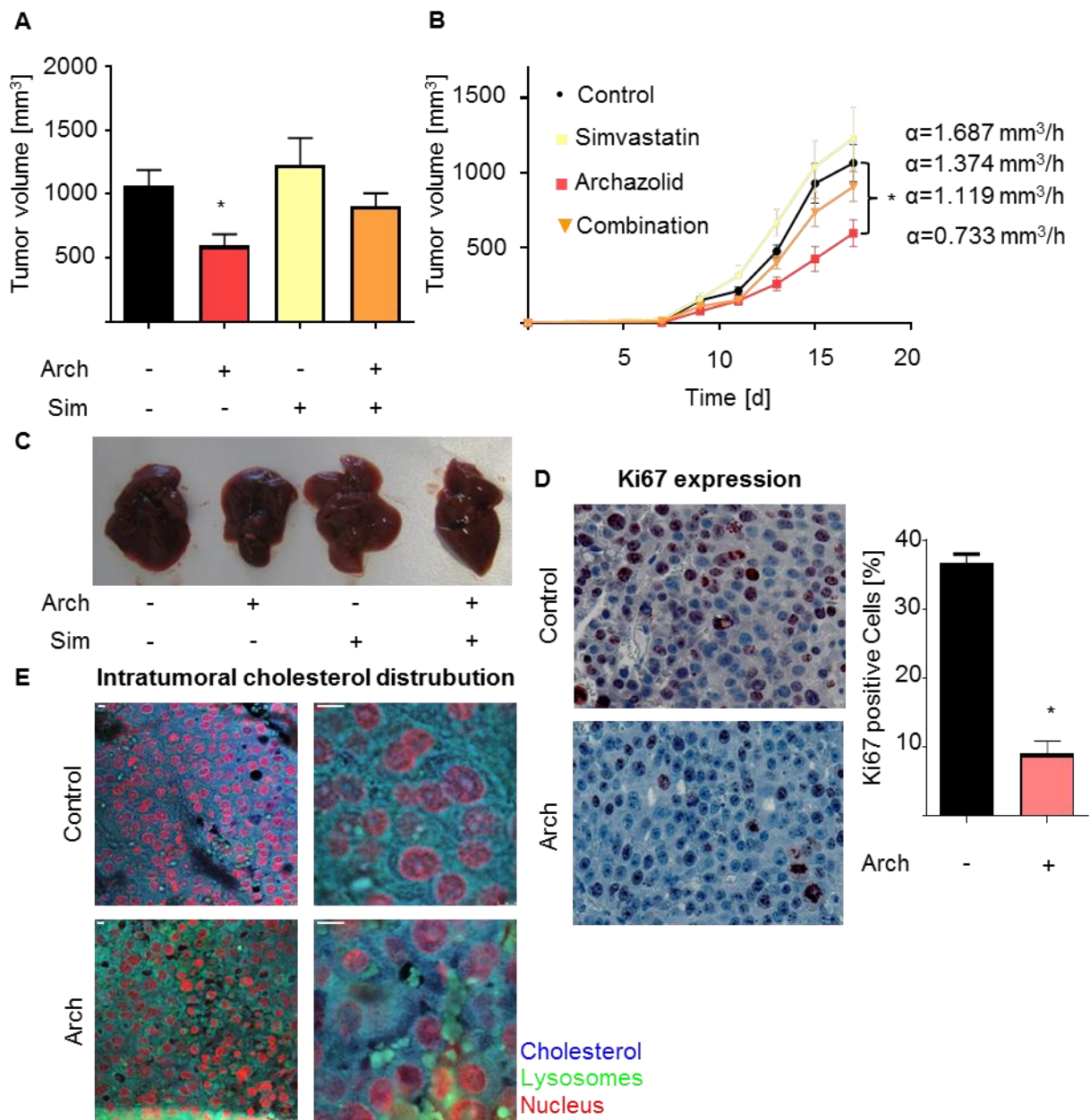


Figure 24 Archazolid leads to reduced proliferation *in vivo* (A, B) HUH-7 cells were injected s.c. into the flanks of 32 SCID mice. Mice were divided in four groups and treated daily i.p. with archazolid, simvastatin, a combination thereof or equal amounts of solvent. Tumor volume (A) and growth rates α (B) (Co $\alpha = 1.374 \text{ mm}^3/\text{h}$, archazolid $\alpha = 0.733 \text{ mm}^3/\text{h}$, simvastatin $\alpha = 1.687 \text{ mm}^3/\text{h}$, combination $\alpha = 1.119 \text{ mm}^3/\text{h}$) are indicated. **(C)** At study end point mice were sacrificed and livers were dissected for visual examination. **(D)** Paraffin sections of tumors were stained for Ki67 and nuclei. **(E)** Paraffin sections of tumors were stained for cholesterol (blue) and LAMP-1 (green). Representative images of control and archazolid treated mice are shown. Scale bar 20 μm . Bars are the mean \pm SEM of three independent experiments. $p < 0.05$ One-way ANOVA, Dunnett post test (A, B) or unpaired t-test (D), respectively

DISCUSSION

4. DISCUSSION

This work reveals that the V-ATPase inhibitor archazolid reduces tumor cell proliferation *in vitro* and *in vivo* by modifying the mechanical phenotype of HCC cells through lysosomal cholesterol trapping, while leaving non-malignant cells unaffected. In an interdisciplinary approach using biophysical and cell-biological methods we were able to identify a new option for the treatment of HCC. Furthermore, we found evidence, that a combination therapy of V-ATPase inhibition with cholesterol synthesis inhibitors might be beneficial.

4.1. The V-ATPase influences membrane properties of the cell - and vice versa?

In the recent past, research mainly focused on directly influencing signaling pathways in order to affect proliferation, invasion and metastasis of cancer cells. Lately however, evidence accumulates that these processes greatly depend on the biomechanical and biophysical aspects of the cells and their environment (67), which opens new possibilities in cancer treatment.

In our study, we show that the HCC cell line HUH-7 is more deformable than the non-malignant hepatocyte cell line HepaRG, indicating increased compliance as a characteristic of liver cancer. These data are in line with the findings of Zhang et al., which reveal differences in elastic coefficients of HCC cells compared to non-malignant tissue and connect them to tumor cell invasion and metastasis (68). Indeed, several studies now exist, which analyzed differences in mechanical phenotype of cancer cells in comparison to their non-malignant counterparts. Along this line, Lin et al. found that different cell lines of breast, bladder, cervical and pancreatic cancer show increased softness when compared to their respective, non-malignant counter-parts. Furthermore, they correlated increased migratory and invasive capability with a loss of sensing and adaption to stiffness changes of the extracellular environment (46). Another study showed a correlation of the softness of tumor cell lines and patient cancer cells with invasiveness and even postulates the use of the mechanical phenotype for grading (69). Moreover, our data show that pharmacological V-ATPase inhibition in HCC cell lines increased cell stiffness compared to untreated cells, while leaving non-malignant cells unaffected, thereby

opening a new possibility for the treatment of HCC by specifically addressing biomechanical properties of liver cancer cells.

We could demonstrate that this effect was due to plasma membrane cholesterol depletion and most likely subsequent disruption of lipid-rafts. Yet, the existence of a loop regulation in this regard is possible, in which the activity of the V-ATPase is further decreased by disruption of lipid-rafts. It has been shown by proteomic analysis, that several subunits of the V-ATPase are depleted from lipid-rafts by cholesterol-disrupting drugs, indicating a raft localization of the proton pump (70). A study by Lafourcade et al. showed that the membrane-integral V-ATPase subunits were associated with detergent resistant membranes, i.e. lipid-raft like domains, isolated from late endosomes. They could show that inducing cholesterol accumulation in late endosomes affected acidification, thereby raising the possibility that association with lipid-raft regulates V-ATPase activity. (71) Another study identified V-ATPase subunits in flotillin 1 enriched triton-insoluble domains of monocytes that can be thought of as lipid-rafts (72). Since it has also been reported, that the activity of the Na⁺/K⁺-ATPase is influenced by membrane cholesterol levels (73), one may hypothesize that the disruption of lipid-rafts by cholesterol depletion caused by V-ATPase inhibition in turn further decreases activity of the proton pump in the fashion of a positive feedback loop. However, the available data are scarce and further studies specifically addressing this matter are needed.

Biophysical properties of the cell are greatly determined by the status of the cytoskeleton, which has been thoroughly studied yet remains unaffected in our study, but also by the plasma membrane composition, of which less is known (74-76). Investigating the membrane properties remains challenging, owing to the complex nature of their composition. Thousands of different lipid species build the backbone of cellular membranes and only due to advances in chromatographic, mass spectrometric and imaging techniques lipid bilayers can now be investigated in more detail. However, satisfying *in vitro* modification options for the plasma membrane composition are still largely missing (64) hence complicating functional membrane studies.

4.2. Cholesterol - an essential factor in cancer cell survival

Cholesterol is a major component of the plasma membrane essentially regulating membrane fluidity, vesicle trafficking, endocytosis and receptor signaling. It has been reported, that cholesterol is crucial for the cytoskeletal adhesion to the plasma membrane in endothelial cells, thereby substantially regulating cell morphology and stiffness - properties that can be influenced by cholesterol depletion (77). In terms of cancer, studies revealed that lipid metabolism is deregulated in different cancers and that aberrant cholesterol metabolism in HCC seems to be a crucial factor in the malignant phenotype (45,66,78,79). In the present study, we could reveal that archazolid selectively reduces free cholesterol levels in HCC cell lines, but not in non-malignant hepatocytes, reinforcing increased compliance and altered lipid metabolism as druggable characteristics of cancer cells in general.

However, the mechanism of cholesterol reprogramming in cancer and subsequent effects still need to be fully examined (48). A study on primary tumor cells and HCC cell lines for instance showed that elevations in overall or mitochondrial cholesterol content were correlated with increased expression of the mitochondrial cholesterol-transporting polypeptide steroidogenic acute regulatory protein (StAR) and chemotherapy resistance together with protection from apoptosis (42). Others reported, that increased mitochondrial cholesterol content due to mutations in the cholesterol export gene ABAC1 also reduced sensitivity to apoptotic signals (80), while contradictory results implicated STARD3, a lipid transfer protein, with poor prognosis in breast cancer (81). Of note, archazolid has been shown by our group to selectively induce apoptosis in tumor cells via induction of intrinsic apoptosis and cellular stress response (12). In context with the relevance of cholesterol for mitochondria, cellular cholesterol depletion as reported in this study might support induction of apoptosis by archazolid.

Cholesterol homeostasis is tightly regulated in cells, by means of synthesis, esterification, metabolism, influx and efflux (34,81,82). The key regulator, that increases cellular cholesterol content is the transcription factor sterol-regulatory element binding protein 2 (SREBP-2), which leads to increased *de novo* synthesis as well as uptake of cholesterol containing lipoproteins and decreased efflux (81). Upon cholesterol depletion sensed by the ER membrane, SREBP-2 is transported to the Golgi for cleavage and subsequently its n-terminal, active form is translocated to the nucleus, where it induces transcription of HMGCR, LDLR and many other genes (34).

Recently, Hamm et al. connected archazolid treatment to an induction of cholesterol metabolism, stating that this is a main resistance mechanism of bladder cancer cells to the treatment (10). In accordance with their data, we found transcriptional induction of SREBP-2, HMGCR and LDLR. However, we draw different conclusions. For one, cholesterol is trapped in the lysosomes leading to depletion of the membrane and thereby alteration of biophysical characteristics and proliferative signaling, which we think is part of the drugs mechanism of action. Additionally, as we show that archazolid blocks LDLR internalization, upregulation of the protein should therefore have no functional consequences. For another, the feedback upregulation of cholesterol synthesis opens the possibility for a combination therapy with statins as discussed below. A combination therapy of archazolid with statins targets cholesterol metabolism in two different ways, thus enabling dose reduction of the single compounds while maintaining or even enhancing therapeutic effectiveness together with reduction of adverse effects.

4.3. Blocking cholesterol uptake and synthesis - a combination therapy as promising anti-cancer strategy

In the present work, we report V-ATPase inhibition as a novel way to achieve restriction of free cholesterol and lipid-raft disruption. As discussed above, alterations in cholesterol metabolism play a major role in cancer but exploitation as therapeutic target still remains challenging. Several different strategies to target aberrant cholesterol metabolism are currently under investigation: targeting cholesterol synthesis, reducing cholesterol uptake, interfering with intracellular cholesterol transport and inhibiting intestinal cholesterol absorption (81). For instance, a preclinical study showed a beneficial effect of ezetimibe, an inhibitor of intestinal cholesterol absorption, on prostate tumor growth (83). Also targeting prenylation by small molecules like an inhibitor of the geranylgeranyltransferase I or disruption of intracellular cholesterol transport by leelamine showed promising results (84,85). Leelamine is a lysosomotropic compound which inhibits cholesterol release from lysosomes and thereby causes membrane cholesterol depletion preferentially in cancer cells (85). In agreement with this finding, we observed that lysosomal trapping of cholesterol leads to a cholesterol depletion of the plasma membrane. We propose that archazolid targets cholesterol uptake by blocking LDL internalization and sequestering cholesterol within the lysosomes, thereby representing a new compound to target cellular cholesterol metabolism.

Extensive research has been done in evaluating the potential role of statins, cholesterol synthesis inhibitors, in cancer treatment, nevertheless the results remain controversial and further studies need to be performed (37,86). In the context of HCC, several studies show beneficial effects of statins either in single treatment or in combination treatment regimens (87). Sutter et al. for instance showed that various statins inhibited the proliferation of HCC by apoptosis induction and cell cycle arrest (88). Interestingly, Yang et al. found in a variety of different cell lines, that atorvastatin inhibits the growth of HCC, yet also induces autophagy as survival mechanism. In a combination therapy approach they blocked autophagy using the V-ATPase inhibitor bafilomycin, thereby enhancing atorvastatin-induced apoptosis (89). Along this line, we show that combining archazolid with simvastatin led to a synergistic enhancement of the anti-proliferative effect of archazolid single treatment. Additionally, apoptosis induction was increased by using the combination treatment. However, these effects were limited to our *in vitro* experiments. In our *in vivo* mouse xenograft model, we surprisingly found slightly induced tumor growth in simvastatin single treated mice and consequently no beneficial effect of a combination treatment. We hypothesize that this finding results from increased angiogenesis caused by simvastatin.

Despite the existence of some pre-clinical studies that propose statins can inhibit tumor growth by reducing angiogenesis (90,91), others report pro-angiogenic properties of statins. Chen et al showed an improved outcome of rats suffering from stroke through administration of statins, which increased VEGF signaling and angiogenesis (92). In another study, Chade et al. showed that statins restore angiogenesis and attenuate intrarenal microvascular remodeling in a pig model for renal ischemia. In their study, simvastatin enhanced both intrarenal angiogenesis and arteriogenesis by increasing angiogenic growth factor expression and hypoxia-inducible factor-1 α signaling (93). Interestingly, a biphasic dose-dependent effect of statins on angiogenesis has been reported by Weis et al. In their study on endothelial cells, they found angiogenesis promoting effects at low therapeutic concentrations but in contrast angiostatic effects at high concentrations. (94) The presence of such a dose-dependency could explain our observation of a clear anti-cancer effect *in vitro*, but not *in vivo*. In our *in vitro* experiments we only assessed the effect of simvastatin on cancer cells, while i.p. administration *in vivo* also targets endothelial cells. We hypothesize that the simvastatin plasma levels in our mouse model favored angiogenesis, which subsequently promoted tumor cell growth in a greater extent

than the growth inhibitory effect on the cancer cells directly. However, further data addressing this discrepancy is needed to draw a final conclusion.

This study and the data of others provide strong experimental evidence for the use of statins to treat HCC, yet like in our mouse model, the situation *in vivo*, especially in humans is vastly more complex. There are several human studies which evaluated the potential effect of statins on the development and treatment of HCC, of which some report a promising statin effect (87,95). However, more randomized controlled trials are necessary to clarify the role of statins in HCC.

In conclusion, our observation of synergistic growth inhibition by targeting the cholesterol metabolism in two ways, together with the research of others strongly suggest that a combination therapy approach might be superior to single agents in the treatment of HCC. Yet, dosage and treatment regimens still need further evaluation.

4.4. Inhibition of Ras signaling - new treatment option for an old oncogene

We report a change in biophysics and cholesterol metabolism upon V-ATPase inhibition, yet to our knowledge little to nothing is known on how this could influence proliferation of human cells. Interestingly, Atilla-Gokcumen et al. recently found first evidence, that cells tightly regulate lipid species and localization during the cell cycle by excessive feedback loops, leading to variations in cell stiffness along the cell cycle (96). This finding raises the question, on whether proliferative signaling is influenced by stiffness alterations. As an essential component of lipid-rafts, cholesterol has already been implicated in the regulation of different signaling pathways in cell survival and apoptosis. Cholesterol depletion in fibroblasts led to an induction of caspase 3 activity and apoptosis via a RhoA and p38 MAPK dependent pathway (49), which goes in line with the finding that Fas and TRAIL dependent apoptosis are lipid-raft dependent in cancer cells (48). Also anoikis-like apoptosis via FAK down-regulation has been observed upon cholesterol depletion and subsequent disruption of caveolae, a sub-type of lipid-rafts. (97). Yet, in our study a different mechanism must be present. On the one hand, we only see mild induction of apoptosis with a maximum of about 25 % in combination treatment with archazolid and simvastatin and on the other hand due to the fact that HUH-7 and HepG2 cells do not express caveolin (98). Additionally, cell survival is greatly determined on growth factor receptor signaling, like the insulin receptor and the EGF receptor (EGFR), which

have been reported to be regulated by cholesterol (44). EGFR dimer formation and the following autophosphorylation of was modulated by cholesterol (44). In an earlier study by our group we could also observe mislocalization of EGFR and a reduction of Rac1 dependent regulation after V-ATPase inhibition (23) however, the effects of cholesterol were not investigated in this study. Noteworthy, EGFR activation leads to an induction of proliferative Ras signaling.

The Ras family of small GTP-ases, was among the first proteins identified with the ability to induce cell growth and soon discovered to be aberrant in tumor cells (50). Ever since, many approaches have been made to specifically target de-regulated Ras signaling, but so far still face major drawbacks. This is caused by the enormous complexity of Ras signaling and activation, which is why Ras is still considered 'undruggable' (99). Major problems in finding small-molecule inhibitors are the high similarity amongst Ras family members and the fact that one Ras protein usually has several regulators, as well as several effectors (100). Yet, a more promising way in targeting Ras might be interfering with Ras localization (99), as it has become evident that different Ras isoforms are targeted to distinct membrane localizations and cause different activation of downstream effectors (52,100,101).

In mammalian cells, three different genes code for four proteins of the Ras family: H-Ras, N-Ras and two different splice variants of K-Ras (K-Ras4A and K-Ras4B) (101). There is significant variation in the contribution of Ras isoforms to the total aberrant Ras activation in different cancer cell lines, however, the major mutated isoform is K-Ras, followed by N-Ras and last H-Ras (102). Nevertheless, in HCC Ras is only mutated in few cases and rather downstream signaling is altered (53,54). Interestingly, there is now evidence that the different isoforms, which have long been thought to signal mainly from plasma membrane locations, are specifically targeted to specific endomembranes and different sites within the plasma membrane and that correct localization is essential to facilitate a variety of downstream signals (52,101). Nevertheless, there is still controversy as to which isoform is located at which membrane and how localization is linked to different downstream signaling (103).

Targeting of Ras to specific membrane sites is achieved by posttranslational modification of the proteins. All three Ras proteins undergo prenylation at their conserved C-terminal CAAX motif (C is cysteine, A is any aliphatic amino acid and X represents any amino acid), leading to ER targeting. N-Ras, H-Ras and K-Ras4A are additionally palmitoylated in the Golgi apparatus and transferred to the plasma

membrane, whereas K-Ras4B does not need additional palmitoylation as its membrane binding is mediated via a polybasic, lysine-rich region. (104) Besides signaling from plasma membrane locations, Ras signaling can also take place on membranes of the Golgi apparatus, the ER and mitochondria each having a different signaling outcome (50,101,105-108). Studies specifically evaluating plasma membrane Ras signaling show that N-Ras and H-Ras are dependent on a functional endocytosis pathway, while K-Ras signaling is not (102,103). In this regard another study reports that EGF activates N-Ras, but not K-Ras, however is enabled to activate both upon cholesterol depletion (100).

We report that upon V-ATPase inhibition the activation of Ras is diminished, leading to impaired downstream signaling namely Raf/MEK/ERK. Yet, we did not distinguish between different Ras isoforms or mutation status. Our study also shows that Ras signaling from plasma membrane lipid-rafts is inhibited by cholesterol depletion as external cholesterol supplementation restored Ras activation. The independence of K-Ras signaling from cholesterol depletion (102,103) might be the reason why the PI3K/Akt pathway in our experiment was not affected though. Yet there is still controversy on which Ras isoforms are more prone to activate Raf-1 or PI3K respectively. While Yan et al. report that K-Ras preferentially induces Raf-1 and H-Ras PI3K (109), Matallanas et al. state that Raf-1 is mainly activated at lipid-rafts (107). So it still has to be clarified which Ras isoform is responsible for the effect we report. Furthermore, cell types with different Ras mutation status should be analyzed to assess, whether our findings provide a therapeutic approach for tumors with specific Ras mutations. Reduced Ras/Raf/MEK/ERK signaling led to a reduction in proliferation *in vitro* and *in vivo* in our experiments, possibly indicating that inhibition of plasma membrane originated Ras signaling is mainly affected as Golgi apparatus dependent Ras signaling has been reported to be insufficient to promote cell proliferation (107).

We think that our results display V-ATPase inhibition as novel option to target lipid-raft dependent Ras signaling ultimately upstream, thereby avoiding specificity and pathway cross talk problems with small molecule inhibitors.

4.5. Concluding remarks and future perspectives

Despite intensive research, new strategies for treatment of HCC are still lacking. While research in the past mostly focused on direct inhibition of oncogenic signaling, targeting cancer cell lipid and cholesterol metabolism, especially in HCC is gaining interest. In the present work, we identified new treatment options for HCC by combining biophysical and cell-biological methods. We demonstrate for the first time that the V-ATPase inhibitor archazolid leads to lysosomal trapping of cholesterol, thereby altering cell stiffness and membrane fluidity. This subsequently leads to decreased proliferation by interference with membrane-related signaling of the well-known oncogene Ras (Fig 25). The *in vivo* efficacy of archazolid in a mouse xenograft HCC model seems to be based on cholesterol trapping as well. Importantly, non-malignant hepatocyte-like cells are not affected by the drug. We propose targeting cholesterol metabolism by V-ATPase-inhibition to be an attractive therapeutic strategy against HCC, which especially might overcome the present challenges in targeting oncogenic Ras signaling.

In a combination therapy approach, we applied the cholesterol synthesis inhibitor simvastatin together with archazolid and could report synergistic inhibition of cell proliferation and induction of apoptosis *in vitro*. Yet, the approach failed to be beneficial in our mouse model, which might be attributed to a pro-angiogenic effect of simvastatin. In conclusion, we think that a combination therapy of archazolid and simvastatin could target cholesterol metabolism and oncogenic Ras signaling in multiple ways and enhance the therapeutic effectiveness (Fig 25). However, future research needs to be done to fine-tune dosage and treatment regimen.

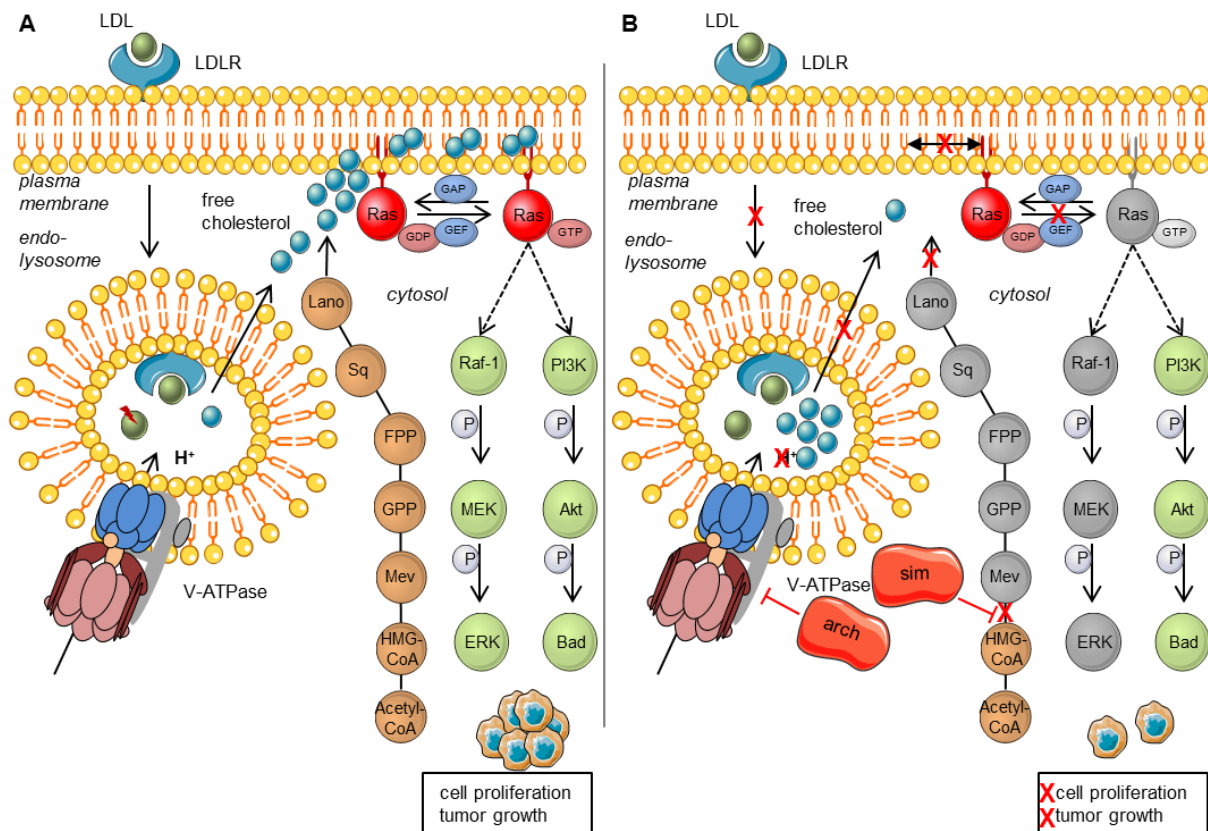


Figure 25 Proposed mechanism of action (A) Under physiological conditions LDL binds to its receptor and is internalized. The V-ATPase acidifies the endo-lysosome, leading to LDL dissociation from the receptor and cleavage. Free cholesterol is then released into the cytosol and is used as building block and for the integration into membranes. Furthermore, cholesterol is synthesized in the cytosol via the mevalonate pathway (brown bullets). Ras is a membrane-bound small GTPase mainly localized in cholesterol-enriched membrane microdomains, where it can be activated. Ras in turn activates different signaling pathways leading to proliferation and tumor growth. **(B)** Upon inhibition of the V-ATPase by Archazolid, LDLR internalization and acidification of the endo-lysosome is inhibited, causing subsequent accumulation of cholesterol within the lysosomes. Due to blocking the conversion of HMG-CoA to mevalonate by simvastatin, *de novo* synthesis of free cholesterol is inhibited. The lack of free cholesterol leads to cholesterol depletion of the membrane and subsequently a disruption of cholesterol-enriched microdomains and a change in membrane properties. As a consequence, cholesterol microdomain-dependent Ras cannot be activated anymore and downstream signaling is inhibited, leading to reduced proliferation and tumor growth. Mev Mevalonate, GPP geranylpyrophosphate, FPP farnesylpyrophosphate, Sq Squalene, Lano Lanosterol, GEF guanosyl-exchange factor, GAP GTPase activating protein, LDL(R) low density lipoprotein (receptor)

REFERENCES

5. REFERENCES

1. El-Serag HB. Hepatocellular carcinoma. *The New England journal of medicine* 2011;365(12):1118-27.
2. Balogh J, Victor D, 3rd, Asham EH, Burroughs SG, Boktour M, Saharia A, et al. Hepatocellular carcinoma: a review. *Journal of hepatocellular carcinoma* 2016;3:41-53.
3. Waller LP, Deshpande V, Prysopoulos N. Hepatocellular carcinoma: A comprehensive review. *World Journal of Hepatology* 2015;7(26):2648-63.
4. Kim JU, Shariff MIF, Crossey MME, Gomez-Romero M, Holmes E, Cox IJ, et al. Hepatocellular carcinoma: Review of disease and tumor biomarkers. *World Journal of Hepatology* 2016;8(10):471-84.
5. Ferlay J SI, Ervik M, Dikshit R, Eser S, Mathers C, Rebelo M, Parkin DM, Forman D, Bray, F. GLOBOCAN 2012 v10, Cancer Incidence and Mortality Worldwide: IARC CancerBase No 11 Lyon, France: International Agency for Research on Cancer; 2013.
6. Lin S, Hoffmann K, Schemmer P. Treatment of hepatocellular carcinoma: a systematic review. *Liver cancer* 2012;1(3-4):144-58.
7. Llovet JM, Ricci S, Mazzaferro V, Hilgard P, Gane E, Blanc JF, et al. Sorafenib in advanced hepatocellular carcinoma. *The New England journal of medicine* 2008;359(4):378-90.
8. Fages A, Duarte-Salles T, Stepien M, Ferrari P, Fedirko V, Pontoizeau C, et al. Metabolomic profiles of hepatocellular carcinoma in a European prospective cohort. *BMC medicine* 2015;13(1):242.
9. Gorin A, Gabitova L, Astsaturov I. Regulation of cholesterol biosynthesis and cancer signaling. *Current opinion in pharmacology* 2012;12(6):710-6.
10. Hamm R, Sugimoto Y, Steinmetz H, Efferth T. Resistance mechanisms of cancer cells to the novel vacuolar H(+)-ATPase inhibitor archazolid B. *Investigational new drugs* 2014;32(5):893-903.
11. Schneider LS, von Schwarzenberg K, Lehr T, Ulrich M, Kubisch-Dohmen R, Liebl J, et al. Vacuolar-ATPase Inhibition Blocks Iron Metabolism to Mediate Therapeutic Effects in Breast Cancer. *Cancer research* 2015;75(14):2863-74.
12. von Schwarzenberg K, Wiedmann RM, Oak P, Schulz S, Zischka H, Wanner G, et al. Mode of cell death induction by pharmacological vacuolar H+-ATPase (V-ATPase) inhibition. *The Journal of biological chemistry* 2013;288(2):1385-96.
13. Schempp CM, von Schwarzenberg K, Schreiner L, Kubisch R, Muller R, Wagner E, et al. V-ATPase inhibition regulates anoikis resistance and metastasis of cancer cells. *Molecular cancer therapeutics* 2014;13(4):926-37.
14. Forgac M. Vacuolar ATPases: rotary proton pumps in physiology and pathophysiology. *Nature reviews Molecular cell biology* 2007;8(11):917-29.
15. Forgac M. Structure, function and regulation of the vacuolar (H+)-ATPases. *FEBS letters* 1998;440(3):258-63.
16. Cotter K, Stransky L, McGuire C, Forgac M. Recent Insights into the Structure, Regulation, and Function of the V-ATPases. *Trends in biochemical sciences* 2015;40(10):611-22.
17. Hinton A, Bond S, Forgac M. V-ATPase functions in normal and disease processes. *Pflugers Archiv : European journal of physiology* 2009;457(3):589-98.
18. Martinez-Zaguilan R, Lynch RM, Martinez GM, Gillies RJ. Vacuolar-type H(+)-ATPases are functionally expressed in plasma membranes of human tumor cells. *The American journal of physiology* 1993;265(4 Pt 1):C1015-29.
19. Sennoune SR, Luo D, Martinez-Zaguilán R. Plasmalemmal vacuolar-type H+-ATPase in cancer biology. *Cell Biochemistry and Biophysics* 2004;40(2):185-206.
20. Cotter K, Capecci J, Sennoune S, Huss M, Maier M, Martinez-Zaguilan R, et al. Activity of plasma membrane V-ATPases is critical for the invasion of MDA-MB231 breast cancer cells. *The Journal of biological chemistry* 2015;290(6):3680-92.

21. Xu J, Xie R, Liu X, Wen G, Jin H, Yu Z, et al. Expression and functional role of vacuolar H⁺-ATPase in human hepatocellular carcinoma. *Carcinogenesis* 2012;33(12):2432-40.
22. Sennoune SR, Bakunts K, Martínez GM, Chua-Tuan JL, Kebir Y, Attaya MN, et al. Vacuolar H⁺-ATPase in human breast cancer cells with distinct metastatic potential: distribution and functional activity. *American Journal of Physiology - Cell Physiology* 2004;286(6):C1443-C52.
23. Wiedmann RM, von Schwarzenberg K, Palamidessi A, Schreiner L, Kubisch R, Liebl J, et al. The V-ATPase-inhibitor archazolid abrogates tumor metastasis via inhibition of endocytic activation of the Rho-GTPase Rac1. *Cancer research* 2012;72(22):5976-87.
24. Hamm R, Chen YR, Seo EJ, Zeino M, Wu CF, Muller R, et al. Induction of cholesterol biosynthesis by archazolid B in T24 bladder cancer cells. *Biochemical pharmacology* 2014;91(1):18-30.
25. Drose S, Bindseil KU, Bowman EJ, Siebers A, Zeeck A, Altendorf K. Inhibitory effect of modified bafilomycins and concanamycins on P- and V-type adenosinetriphosphatases. *Biochemistry* 1993;32(15):3902-6.
26. Dröse S, Altendorf K. Bafilomycins and concanamycins as inhibitors of V-ATPases and P-ATPases. *The Journal of experimental biology* 1997;200(1):1-8.
27. Huss M, Wieczorek H. Inhibitors of V-ATPases: old and new players. *The Journal of experimental biology* 2009;212(Pt 3):341-6.
28. Gagliardi S, Gatti PA, Belfiore P, Zocchetti A, Clarke GD, Farina C. Synthesis and Structure–Activity Relationships of Bafilomycin A1 Derivatives as Inhibitors of Vacuolar H⁺-ATPase. *Journal of Medicinal Chemistry* 1998;41(11):1883-93.
29. Páli T, Whyteside G, Dixon N, Kee TP, Ball S, Harrison MA, et al. Interaction of Inhibitors of the Vacuolar H⁺-ATPase with the Transmembrane Vo-Sector. *Biochemistry* 2004;43(38):12297-305.
30. Reichenbach H, Hofle G. Biologically active secondary metabolites from myxobacteria. *Biotechnology advances* 1993;11(2):219-77.
31. Sasse F, Steinmetz H, Hofle G, Reichenbach H. Archazolids, new cytotoxic macrolactones from *Archangium gephyra* (Myxobacteria). Production, isolation, physico-chemical and biological properties. *The Journal of antibiotics* 2003;56(6):520-5.
32. Menche D, Hassfeld J, Li J, Rudolph S. Total synthesis of archazolid A. *Journal of the American Chemical Society* 2007;129(19):6100-1.
33. Roethle PA, Chen IT, Trauner D. Total Synthesis of (–)-Archazolid B. *Journal of the American Chemical Society* 2007;129(29):8960-61.
34. Ikonen E. Cellular cholesterol trafficking and compartmentalization. *Nature reviews Molecular cell biology* 2008;9(2):125-38.
35. Goedeke L, Fernandez-Hernando C. Regulation of cholesterol homeostasis. *Cellular and molecular life sciences : CMLS* 2012;69(6):915-30.
36. Thurnher M, Nussbaumer O, Gruenbacher G. Novel Aspects of Mevalonate Pathway Inhibitors as Antitumor Agents. *Clinical Cancer Research* 2012;18(13):3524-31.
37. Demierre MF, Higgins PD, Gruber SB, Hawk E, Lippman SM. Statins and cancer prevention. *Nature reviews Cancer* 2005;5(12):930-42.
38. Kuoppala J, Lamminpää A, Pukkala E. Statins and cancer: A systematic review and meta-analysis. *European journal of cancer (Oxford, England : 1990)* 2008;44(15):2122-32.
39. Grundy SM. Absorption and metabolism of dietary cholesterol. *Annual review of nutrition* 1983;3:71-96.
40. Byfield FJ, Aranda-Espinoza H, Romanenko VG, Rothblat GH, Levitan I. Cholesterol depletion increases membrane stiffness of aortic endothelial cells. *Biophysical journal* 2004;87(5):3336-43.
41. Ohvo-Rekilä H, Ramstedt B, Leppimäki P, Peter Slotte J. Cholesterol interactions with phospholipids in membranes. *Progress in Lipid Research* 2002;41(1):66-97.

42. Montero J, Morales A, Llacuna L, Lluís JM, Terrones O, Basanez G, et al. Mitochondrial cholesterol contributes to chemotherapy resistance in hepatocellular carcinoma. *Cancer research* 2008;68(13):5246-56.
43. Maxfield FR, Wustner D. Intracellular cholesterol transport. *The Journal of clinical investigation* 2002;110(7):891-8.
44. Pike LJ. Growth factor receptors, lipid rafts and caveolae: an evolving story. *Biochimica et biophysica acta* 2005;1746(3):260-73.
45. Staubach S, Hanisch FG. Lipid rafts: signaling and sorting platforms of cells and their roles in cancer. *Expert review of proteomics* 2011;8(2):263-77.
46. Lin HH, Lin HK, Lin IH, Chiou YW, Chen HW, Liu CY, et al. Mechanical phenotype of cancer cells: cell softening and loss of stiffness sensing. *Oncotarget* 2015;6(25):20946-58.
47. Montero J, Morales A, Llacuna L, Lluís JM, Terrones O, Basañez G, et al. Mitochondrial Cholesterol Contributes to Chemotherapy Resistance in Hepatocellular Carcinoma. *Cancer Research* 2008;68(13):5246-56.
48. Cruz PM, Mo H, McConathy WJ, Sabnis N, Lacko AG. The role of cholesterol metabolism and cholesterol transport in carcinogenesis: a review of scientific findings, relevant to future cancer therapeutics. *Frontiers in pharmacology* 2013;4:119.
49. Calleros L, Lasa M, Rodriguez-Alvarez FJ, Toro MJ, Chiloeches A. RhoA and p38 MAPK mediate apoptosis induced by cellular cholesterol depletion. *Apoptosis : an international journal on programmed cell death* 2006;11(7):1161-73.
50. Downward J. Targeting RAS signalling pathways in cancer therapy. *Nature reviews Cancer* 2003;3(1):11-22.
51. Whittaker S, Marais R, Zhu AX. The role of signaling pathways in the development and treatment of hepatocellular carcinoma. *Oncogene* 2010;29(36):4989-5005.
52. Hancock JF. Ras proteins: different signals from different locations. *Nature reviews Molecular cell biology* 2003;4(5):373-84.
53. Delire B, Starkel P. The Ras/MAPK pathway and hepatocarcinoma: pathogenesis and therapeutic implications. *European journal of clinical investigation* 2015;45(6):609-23.
54. Llovet JM, Bruix J. Molecular targeted therapies in hepatocellular carcinoma. *Hepatology (Baltimore, Md)* 2008;48(4):1312-27.
55. Owen DM, Rentero C, Magenau A, Abu-Siniyeh A, Gaus K. Quantitative imaging of membrane lipid order in cells and organisms. *Nature protocols* 2012;7(1):24-35.
56. Schieder M, Rotzer K, Bruggemann A, Biel M, Wahl-Schott C. Planar patch clamp approach to characterize ionic currents from intact lysosomes. *Science signaling* 2010;3(151):pl3.
57. Koeberle A, Pergola C, Shindou H, Koeberle SC, Shimizu T, Laufer SA, et al. Role of p38 mitogen-activated protein kinase in linking stearoyl-CoA desaturase-1 activity with endoplasmic reticulum homeostasis. *FASEB journal : official publication of the Federation of American Societies for Experimental Biology* 2015;29(6):2439-49.
58. Nicoletti I, Migliorati G, Pagliacci MC, Grignani F, Riccardi C. A rapid and simple method for measuring thymocyte apoptosis by propidium iodide staining and flow cytometry. *Journal of immunological methods* 1991;139(2):271-9.
59. Otto O, Rosendahl P, Mietke A, Golfier S, Herold C, Klau D, et al. Real-time deformability cytometry: on-the-fly cell mechanical phenotyping. *Nature methods* 2015;12(3):199-202, 4 p following 02.
60. Mietke A, Otto O, Girardo S, Rosendahl P, Taubenberger A, Golfier S, et al. Extracting Cell Stiffness from Real-Time Deformability Cytometry: Theory and Experiment. *Biophysical journal* 2015;109(10):2023-36.
61. Smith PK, Krohn RI, Hermanson GT, Mallia AK, Gartner FH, Provenzano MD, et al. Measurement of protein using bicinchoninic acid. *Analytical biochemistry* 1985;150(1):76-85.
62. Ladner CL, Yang J, Turner RJ, Edwards RA. Visible fluorescent detection of proteins in polyacrylamide gels without staining. *Analytical biochemistry* 2004;326(1):13-20.

63. Fleige S, Walf V, Huch S, Prgomet C, Sehm J, Pfaffl MW. Comparison of relative mRNA quantification models and the impact of RNA integrity in quantitative real-time RT-PCR. *Biotechnology letters* 2006;28(19):1601-13.
64. Muro E, Atilla-Gokcumen GE, Eggert US. Lipids in cell biology: how can we understand them better? *Molecular biology of the cell* 2014;25(12):1819-23.
65. Owen DM, Gaus K. Imaging lipid domains in cell membranes: the advent of super-resolution fluorescence microscopy. *Frontiers in plant science* 2013;4:503.
66. Head BP, Patel HH, Insel PA. Interaction of membrane/lipid rafts with the cytoskeleton: impact on signaling and function: membrane/lipid rafts, mediators of cytoskeletal arrangement and cell signaling. *Biochimica et biophysica acta* 2014;1838(2):532-45.
67. Fenner J, Stacer AC, Winterroth F, Johnson TD, Luker KE, Luker GD. Macroscopic stiffness of breast tumors predicts metastasis. *Scientific reports* 2014;4:5512.
68. Zhang G, Long M, Wu ZZ, Yu WQ. Mechanical properties of hepatocellular carcinoma cells. *World journal of gastroenterology : WJG* 2002;8(2):243-6.
69. Swaminathan V, Mythreye K, O'Brien ET, Berchuck A, Blobe GC, Superfine R. Mechanical stiffness grades metastatic potential in patient tumor cells and in cancer cell lines. *Cancer research* 2011;71(15):5075-80.
70. Foster LJ, De Hoog CL, Mann M. Unbiased quantitative proteomics of lipid rafts reveals high specificity for signaling factors. *Proceedings of the National Academy of Sciences of the United States of America* 2003;100(10):5813-8.
71. Lafourcade C, Sobo K, Kieffer-Jaquinod S, Garin J, van der Goot FG. Regulation of the V-ATPase along the Endocytic Pathway Occurs through Reversible Subunit Association and Membrane Localization. *PloS one* 2008;3(7):e2758.
72. Li N, Mak A, Richards DP, Naber C, Keller BO, Li L, et al. Monocyte lipid rafts contain proteins implicated in vesicular trafficking and phagosome formation. *Proteomics* 2003;3(4):536-48.
73. Barenholz Y. Cholesterol and other membrane active sterols: from membrane evolution to "rafts". *Progress in Lipid Research* 2002;41(1):1-5.
74. Guck J, Schinkinger S, Lincoln B, Wottawah F, Ebert S, Romeyke M, et al. Optical deformability as an inherent cell marker for testing malignant transformation and metastatic competence. *Biophysical journal* 2005;88(5):3689-98.
75. Fletcher DA, Mullins RD. Cell mechanics and the cytoskeleton. *Nature* 2010;463(7280):485-92.
76. Fuhrmann A, Staunton JR, Nandakumar V, Banyai N, Davies PCW, Ros R. AFM stiffness nanotomography of normal, metaplastic and dysplastic human esophageal cells. *Physical biology* 2011;8(1):015007-07.
77. Sun M, Northup N, Marga F, Huber T, Byfield FJ, Levitan I, et al. The effect of cellular cholesterol on membrane-cytoskeleton adhesion. *Journal of cell science* 2007;120(Pt 13):2223-31.
78. Santos CR, Schulze A. Lipid metabolism in cancer. *The FEBS journal* 2012;279(15):2610-23.
79. Morales A, Mari M, Garcia-Ruiz C, Colell A, Fernandez-Checa JC. Hepatocarcinogenesis and ceramide/cholesterol metabolism. *Anti-cancer agents in medicinal chemistry* 2012;12(4):364-75.
80. Smith B, Land H. Anticancer activity of the cholesterol exporter ABCA1 gene. *Cell reports* 2012;2(3):580-90.
81. Kuzu OF, Noory MA, Robertson GP. The Role of Cholesterol in Cancer. *Cancer research* 2016;76(8):2063-70.
82. Hullin-Matsuda F, Taguchi T, Greimel P, Kobayashi T. Lipid compartmentalization in the endosome system. *Seminars in cell & developmental biology* 2014;31:48-56.
83. Solomon KR, Pelton K, Boucher K, Joo J, Tully C, Zurakowski D, et al. Ezetimibe Is an Inhibitor of Tumor Angiogenesis. *The American journal of pathology* 2009;174(3):1017-26.
84. Ginestier C, Monville F, Wicinski J, Cabaud O, Cervera N, Josselin E, et al. Mevalonate metabolism regulates Basal breast cancer stem cells and is a potential therapeutic target. *Stem cells (Dayton, Ohio)* 2012;30(7):1327-37.

85. Kuzu OF, Gowda R, Sharma A, Robertson GP. Leelamine mediates cancer cell death through inhibition of intracellular cholesterol transport. *Molecular cancer therapeutics* 2014;13(7):1690-703.
86. Brown AJ. Cholesterol, statins and cancer. *Clinical and experimental pharmacology & physiology* 2007;34(3):135-41.
87. Lonardo A, Loria P. Potential for statins in the chemoprevention and management of hepatocellular carcinoma. *Journal of gastroenterology and hepatology* 2012;27(11):1654-64.
88. Sutter AP, Maaser K, Hopfner M, Huether A, Schuppan D, Scherubl H. Cell cycle arrest and apoptosis induction in hepatocellular carcinoma cells by HMG-CoA reductase inhibitors. Synergistic antiproliferative action with ligands of the peripheral benzodiazepine receptor. *Journal of hepatology* 2005;43(5):808-16.
89. Yang PM, Liu YL, Lin YC, Shun CT, Wu MS, Chen CC. Inhibition of autophagy enhances anticancer effects of atorvastatin in digestive malignancies. *Cancer research* 2010;70(19):7699-709.
90. Gao J, Jia WD, Li JS, Wang W, Xu GL, Ma JL, et al. Combined inhibitory effects of celecoxib and fluvastatin on the growth of human hepatocellular carcinoma xenografts in nude mice. *The Journal of international medical research* 2010;38(4):1413-27.
91. Tijeras-Raballand A, Hainaud-Hakim P, Contreres J-O, Gest C, Le Henaff C, et al. Rosuvastatin Counteracts Vessel Arterialisation and Sinusoid Capillarisation, Reduces Tumour Growth, and Prolongs Survival in Murine Hepatocellular Carcinoma. *Gastroenterology Research and Practice* 2010;2010:14.
92. Chen J, Zhang ZG, Li Y, Wang Y, Wang L, Jiang H, et al. Statins induce angiogenesis, neurogenesis, and synaptogenesis after stroke. *Annals of neurology* 2003;53(6):743-51.
93. Chade AR, Zhu X, Mushin OP, Napoli C, Lerman A, Lerman LO. Simvastatin promotes angiogenesis and prevents microvascular remodeling in chronic renal ischemia. *FASEB journal : official publication of the Federation of American Societies for Experimental Biology* 2006;20(10):1706-8.
94. Weis M, Heeschen C, Glassford AJ, Cooke JP. Statins Have Biphasic Effects on Angiogenesis. *Circulation* 2002;105(6):739-45.
95. El-Serag HB, Johnson ML, Hachem C, Morgana RO. Statins are associated with a reduced risk of hepatocellular carcinoma in a large cohort of patients with diabetes. *Gastroenterology* 2009;136(5):1601-8.
96. Atilla-Gokcumen GE, Muro E, Relat-Goberna J, Sasse S, Bedigian A, Coughlin ML, et al. Dividing cells regulate their lipid composition and localization. *Cell* 2014;156(3):428-39.
97. Park EK, Park MJ, Lee SH, Li YC, Kim J, Lee JS, et al. Cholesterol depletion induces anoikis-like apoptosis via FAK down-regulation and caveolae internalization. *The Journal of pathology* 2009;218(3):337-49.
98. Cokakli M, Erdal E, Nart D, Yilmaz F, Sagol O, Kilic M, et al. Differential expression of Caveolin-1 in hepatocellular carcinoma: correlation with differentiation state, motility and invasion. *BMC cancer* 2009;9:65.
99. Schmick M, Kraemer A, Bastiaens PI. Ras moves to stay in place. *Trends in cell biology* 2015;25(4):190-7.
100. Kranenburg O, Verlaan I, Moolenaar WH. Regulating c-Ras function. cholesterol depletion affects caveolin association, GTP loading, and signaling. *Current biology : CB* 2001;11(23):1880-4.
101. Fehrenbacher N, Bar-Sagi D, Philips M. Ras/MAPK signaling from endomembranes. *Molecular oncology* 2009;3(4):297-307.
102. Omerovic J, Hammond DE, Clague MJ, Prior IA. Ras isoform abundance and signalling in human cancer cell lines. *Oncogene* 2008;27(19):2754-62.
103. Bivona TG, Philips MR. Ras pathway signaling on endomembranes. *Current opinion in cell biology* 2003;15(2):136-42.

104. Konstantinopoulos PA, Karamouzis MV, Papavassiliou AG. Post-translational modifications and regulation of the RAS superfamily of GTPases as anticancer targets. *Nature reviews Drug discovery* 2007;6(7):541-55.
105. Hancock JF. Ras proteins: different signals from different locations. *Nat Rev Mol Cell Biol* 2003;4(5):373-85.
106. McCubrey JA, Steelman LS, Chappell WH, Abrams SL, Wong EW, Chang F, et al. Roles of the Raf/MEK/ERK pathway in cell growth, malignant transformation and drug resistance. *Biochimica et biophysica acta* 2007;1773(8):1263-84.
107. Matallanas D, Sanz-Moreno V, Arozarena I, Calvo F, Agudo-Ibanez L, Santos E, et al. Distinct utilization of effectors and biological outcomes resulting from site-specific Ras activation: Ras functions in lipid rafts and Golgi complex are dispensable for proliferation and transformation. *Molecular and cellular biology* 2006;26(1):100-16.
108. Lynch SJ, Snitkin H, Gumper I, Philips MR, Sabatini D, Pellicer A. The differential palmitoylation states of N-Ras and H-Ras determine their distinct Golgi subcompartment localizations. *Journal of cellular physiology* 2015;230(3):610-9.
109. Yan J, Roy S, Apolloni A, Lane A, Hancock JF. Ras isoforms vary in their ability to activate Raf-1 and phosphoinositide 3-kinase. *The Journal of biological chemistry* 1998;273(37):24052-6.
110. Bartel K, Winzi M, Ulrich M, Koeberle A, Menche D, Werz O, et al. V-ATPase inhibition increases cancer cell stiffness and blocks membrane related Ras signaling - a new option for HCC therapy. *Oncotarget* 2016.
111. Nguyen ONP, Grimm C, Schneider LS, Chao Y-K, Atzberger C, Bartel K, et al. Two-pore channel function is crucial for migration of invasive cancer cells. *Cancer research* 2017.

APPENDIX

6. APPENDIX

6.1. Abbreviations

°C	degree Celsius
µg/mg/kg	micro/milli/kilo gram(s)
µl/ml	micro/milli liter(s)
Akt	protein kinase B
arch	archazolid
ATP	adenosine triphosphate
Bad	Bcl-2-antagonist of cell death
BC	bichinchonic acid
BSA	bovine serum albumine
CE	cholesteryl ester
CO ₂	carbon dioxide
CoA	coenzyme A
d	day(s)
DMEM	dulbecco's modified eagle medium
DMSO	dimethylsulfoxide
DNA	desoxyribonucleic acid
DTT	dithiothreitol
ECL	enhanced chemiluminescence
EDTA	ethylenediaminetetraacetic acid
EGF(R)	epidermal growth factor (receptor)
EGTA	ethylene glycol-bis(β-aminoethyl ether)-N,N,N',N'-tetraacetic acid
ER	endoplasmatic reticulum
ERK	extracellular signal-regulated kinase
FAK	focal adhesion kinase
Fas	a transmembrane protein of the tumor necrosis factor family
FCS	fetal calf serum
FRAP	fluorescence recovery after photo-bleaching
g	gravity
Ga	gauge
GAP	GTP-ase activating protein
GDP	guanosine diphosphate

GEF	guanosyl-exchange factor
GFP	green fluorescent protein
GP	generalized polarization
GRB2	Growth factor receptor-bound protein 2
GTP	guanosine triphosphate
h	hour(s)
H ₂ O ₂	hydrogen peroxide
HCC	hepatocellular carcinoma
Hep3B	liver cancer cell line
HepG2	liver cancer cell line
hHep	primary human hepatocytes
HMG-CoA	3-Hydroxy-3-Methylglutaryl-CoA
HMGCR	3-Hydroxy-3-Methylglutaryl-CoA reductase
Hoechst	Hoechst 33342, bisBenzimide
HRP	horseradish peroxidase
HUH-7	liver cancer cell line
i.p.	intra peritoneal
IHC	immune histochemistry
LAMP-1	lysosomal-associated membrane protein 1
LDL (R)	low density lipoprotein (receptor)
LX-R	liver X receptor
MEK	mitogen-activated protein kinase kinase
min	minute(s)
mRNA	messenger RNA
n/cm	nano/centi meter(s)
Na ₃ VO ₄	sodium orthovanadate
NaCl	sodium chloride
NaF	sodium fluoride
nM/μM/mM	nano/micro/milli molar
P	phosphate
P/S	penicillin streptomycin
p38 MAPK	p38 mitogen-activated protein kinase
PBS	phosphate buffered saline
PFA	para formaldehyde

PI	propidium iodide
PI3K	phosphoinositide 3-kinase
PLC ϵ	1-Phosphatidylinositol-4,5-bisphosphate phosphodiesterase epsilon
PMA	phorbol myristate acetate
PMSF	phenylmethylsulfonylfluorid
PP	pyrophosphate
qPCR	quantitative real-time polymerase chain reaction
Raf	rapidly accelerated fibrosarcoma or rat fibrosarcoma
RalGDS	Ral guanine nucleotide dissociation stimulator
Ras	rat sarcoma
RhoA	Ras homolog gene family member A
RNA	ribonucleic acid
rpm	rotations per minute
RT-DC	real-time deformability cytometry
s	second(s)
SCID	severe combined immune deficiency
SDS	sodium dodecyl sulfate
siRNA	small-interfering RNA
SOS	son of sevenless
SREBP-2	sterol-regulatory element binding protein 2
STR	short tandem repeat
TCE	trichloroethanol
TRAIL	tumor necrosis factor related apoptosis inducing ligand
U/ml	unit per milliliter
V-ATPase	vacuolar-type ATPase
VLDL	very low density lipoprotein
w/v	weight per volume

6.2. Publications

6.2.1. Articles

Karin Bartel, Maria Winzi, Melanie Ulrich, Andreas Koeberle, Dirk Menche, Oliver Werz, Rolf Müller, Jochen Guck, Angelika M. Vollmar, Karin von Schwarzenberg, “*V-ATPase inhibition increases cancer cell stiffness and blocks membrane related - Ras signaling - a new option for HCC therapy*“, 2016, Oncotarget (110)

Ong Nam Phuong Nguyen, Christian Grimm, Lina S. Schneider, Yu-Kai Chao, Carina Atzberger, **Karin Bartel**, Anna Watermann, Melanie Ulrich, Doris Mayr, Christian Wahl-Schott, Martin Biel, Angelika M. Vollmar, “*Two-pore channel function is crucial for migration of invasive cancer cells*“, 2017, Cancer Research (111)

6.2.2. Oral presentations

Karin Steiner, Angelika M. Vollmar, Karin von Schwarzenberg, “*V-ATPase inhibition by archazolid A influences cholesterol metabolism of cancer cells*“, 2nd European Conference on Natural Products, September 6-9th, 2015, Frankfurt, Germany

Karin Steiner, Angelika M. Vollmar, Karin von Schwarzenberg, “*Effect of Archazolid A on metabolism in HCC*“, FOR 1406 Meeting, June 30th - July 1st, 2015, Saarbrücken, Germany

Karin Steiner, Angelika M. Vollmar, Karin von Schwarzenberg, “*Effect of Archazolid A on metabolism in hepatocellular carcinoma cell lines*“, FOR 1406 Meeting, January 8-9th, 2015, Munich, Germany

6.2.3. Poster presentations

Karin Bartel, Maria Winzi, Melanie Ulrich, Andreas Koeberle, Dirk Menche, Oliver Werz, Rolf Müller, Jochen Guck, Angelika M. Vollmar, Karin von Schwarzenberg, “*V-ATPase inhibition influences cholesterol metabolism of cancer cells – a new option for HCC therapy*“, Metabolic networks in cancer, 3rd annual meeting of the ISCaM society, October 26-29th, 2016, Brussels, Belgium

Karin Bartel, Maria Winzi, Melanie Ulrich, Andreas Koeberle, Dirk Menche, Oliver Werz, Rolf Müller, Jochen Guck, Angelika M. Vollmar, Karin von Schwarzenberg, “*Targeting cholesterol metabolism in hepatocellular carcinoma - V-ATPase inhibition as a novel therapeutic option*“, DPHG annual meeting 2016, October 4-6th, 2016, Munich, Germany

Karin Steiner, Rolf Müller, Angelika M. Vollmar, Karin von Schwarzenberg, “*V-ATPase inhibition by Archazolid A influences cholesterol metabolism of cancer cells*“, HIPS Symposium, July 2nd, 2015, Saarbrücken, Germany

Karin Steiner, Rolf Müller, Angelika M. Vollmar, Karin von Schwarzenberg, “*V-ATPase inhibition influences cholesterol metabolism of cancer cells*“, V-ATPase symposium, May 14-15th, 2015, Milan, Italy

Karin Steiner, Angelika M. Vollmar, Karin von Schwarzenberg, "*V-ATPase inhibition by Archazolid A influences cholesterol metabolism of cancer cells*", Interact 2015, March 8th, 2015, Munich, Germany

Karin Steiner, Angelika M. Vollmar, Karin von Schwarzenberg, "*Synergistic effects of Archazolid A and Simvastatin on hepatocellular carcinoma cells*", Graduate School of Natural Product Research Summer Symposium, July 9th, 2014, Saarbrücken, Germany

6.3. Acknowledgements

Mein größter Dank gilt Frau Professor Vollmar für die Möglichkeit meine Doktorarbeit an Ihrem Lehrstuhl anfertigen zu können. Ich möchte mich für Ihr anhaltendes Vertrauen und die ausgezeichneten Ratschläge, sowohl in fachlichen, als auch in persönlichen Angelegenheiten bedanken. Mit Ihrem Eifer für die Wissenschaft und die Lehre sind Sie für mich ein großes Vorbild.

Ein besonderer Dank gilt natürlich meinen weiteren Prüfern. Vielen Dank Hanna, dass du meine Arbeit als 2. Gutachterin beurteilt hast. Außerdem auch für die Betreuung meines Forschungspraktikums in einer für mich schweren Zeit, das mich in der Überzeugung gestärkt hat promovieren zu wollen und für die zahlreichen Gespräche über unsere gemeinsame Leidenschaft, den Sport.

Einen großen Dank auch an Prof. Dr. Christian Wahl-Schott und Prof. Dr. Ernst Wagner für Ihre Rolle als Dritt- und Viertprüfer. Danke auch an Herrn PD Dr. Michalakis und Prof. Dr. Franz Paintner, als Fünft- und Sechstprüfer für das Interesse an meiner Arbeit.

Ganz herzlich möchte ich mich bei Karin bedanken. Liebe Karin, vielen Dank für die hervorragende Betreuung während meiner Zeit in unserem kleinen Team Karin. Deine Tür stand mir immer offen, sowohl für fachliche Diskussionen, als auch für private Probleme oder Sorgen. Danke auch für dein Vertrauen und die großen Freiheiten, in der Gestaltung meiner Arbeit. Du bist für mich wissenschaftlich und auch privat ein sehr großes Vorbild.

Ein großer Dank gilt auch allen Mitarbeitern unseres Arbeitskreises. Es herrschte immer ein offenes und sehr gutes Betriebsklima, das keinen Falls selbstverständlich ist. Die gute Stimmung und das gute Verhältnis erstreckte sich auch weit über die Arbeit hinaus in die Freizeit, was es jeden Morgen umso einfacher machte in die Arbeit und gleichzeitig zu Freunden zu gehen. Besonders lieben Dank an dieser Stelle an Fabi, Meli und Chrissi für die tolle Zeit im Studium, im Labor und bei so vielen tollen Erlebnissen außerhalb. Danke auch Flo und Max für die schöne Zeit. Vielen Dank an Herrn Prof. Zahler für kritischen Diskussionen und die hervorragende Unterstützung, vor allem bei technischen Problemen. Vielen Dank auch an Jana, dass du mir als Neuling im Labor alles geduldig gezeigt hast und mir bei jedem Problem immer geholfen hast.

Last, but not least: An dieser Stelle möchte ich mich bei meiner Familie und meinem Mann bedanken.

Liebe Mama, eigentlich fehlen mir die Worte, um meinen Dank auszudrücken. Danke für deine grenzenlose Unterstützung vom Kindergarten bis zum Studium. Besonders in unseren schwersten Zeiten als wir Sigi verloren und deine Erkrankung überstanden haben, warst du für mich nicht nur Mama, sondern auch immer beste Freundin.

Lieber Erwin, danke für alles. Vor allem dafür, dass wir uns eigentlich nie gestritten haben und du mir bei allen Problemen zur Seite gestanden hast. Auch dass du mich mit deinem Programmier-Wissen und deinem physikalischen Verständnis in einigen Aspekten meiner Doktorarbeit sehr viel weiter gebracht hast.

Lieber Domi, danke. Dafür, dass du seit dem Studium immer an meiner Seite warst, dass du mit mir die intensivsten Lernphasen verbracht hast, wir zusammen unser Studium gemeistert haben und dass du auch während meiner Doktorarbeit immer noch ein Ohr für meine fachlichen Probleme hattest. Danke dass du mein Anker in den schwersten Zeiten meines Lebens warst, dass du mich immer wieder aufgefangen hast und dass wir auch unsere Zukunft gemeinsam verbringen werden. In guten, wie in schweren Tagen.

Danke, dass ihr immer an mich geglaubt und mich unterstützt habt, ohne euch wäre das alles nicht möglich gewesen!